The Journal of Chemical Physics

Extensions of the worm-like-chain model to tethered active filaments under tension

Cite as: J. Chem. Phys. **153**, 194901 (2020); https://doi.org/10.1063/5.0025200
Submitted: 13 August 2020 • Accepted: 26 October 2020 • Published Online: 17 November 2020

Xinyu Liao, Prashant K. Purohit and Arvind Gopinath

AIP Publishing

The Journal of Chemical Physics ARTICLE scitation.org/journal/jcp

Extensions of the worm-like-chain model to tethered active filaments under tension

Cite as: J. Chem. Phys. 153, 194901 (2020); doi: 10.1063/5.0025200
Submitted: 13 August 2020 • Accepted: 26 October 2020 •
Published Online: 17 November 2020

Xinyu Liao,[1,a)] Prashant K. Purohit,[1,2,b)] and Arvind Gopinath[3,c)]

AFFILIATIONS

[1]Graduate Group in Applied Mathematics and Computational Science, University of Pennsylvania, Philadelphia, Pennsylvania 19104, USA
[2]Department of Mechanical Engineering and Applied Mechanics, University of Pennsylvania, Philadelphia, Pennsylvania 19104, USA
[3]Department of Bioengineering, University of California Merced, Merced, California 95343, USA

[a)]**Electronic mail:** xinyul@sas.upenn.edu
[b)]**Electronic mail:** purohit@seas.upenn.edu
[c)]**Author to whom correspondence should be addressed:** agopinath@ucmerced.edu

ABSTRACT

Intracellular elastic filaments such as microtubules are subject to thermal Brownian noise and active noise generated by molecular motors that convert chemical energy into mechanical work. Similarly, polymers in living fluids such as bacterial suspensions and swarms suffer bending deformations as they interact with single bacteria or with cell clusters. Often, these filaments perform mechanical functions and interact with their networked environment through cross-links or have other similar constraints placed on them. Here, we examine the mechanical properties—under tension—of such constrained active filaments under canonical boundary conditions motivated by experiments. Fluctuations in the filament shape are a consequence of two types of random forces—thermal Brownian forces and activity derived forces with specified time and space correlation functions. We derive force-extension relationships and expressions for the mean square deflections for tethered filaments under various boundary conditions including hinged and clamped constraints. The expressions for hinged–hinged boundary conditions are reminiscent of the worm-like-chain model and feature effective bending moduli and mode-dependent non-thermodynamic effective temperatures controlled by the imposed force and by the activity. Our results provide methods to estimate the activity by measurements of the force-extension relation of the filaments or their mean square deflections, which can be routinely performed using optical traps, tethered particle experiments, or other single molecule techniques.

I. INTRODUCTION

The structural elasticity of slender biofilaments and polymers such as DNA, proteins, actin, and microtubules and their deformation in response to their environment are key to their function.[1–16] In a homogeneous medium at constant temperature, embedded filaments and polymers suffer stochastic bending fluctuations. These deformations arise due to the action of thermal Brownian random forces on the filament. In passive settings, the energy to create a curved segment of the filament is drawn from the ambient bath; conversely, already curved segments of the filament flatten by viscous dissipation of stored energy into the medium. At equilibrium, this dual role of the thermal bath and the statistical properties of the forcing manifests in the fluctuation-dissipation theorem that relates the magnitudes of the delta-correlated forces with the thermodynamic temperature T.[10,17–19]

In this work, we study the properties of fluctuating elastic filaments under active settings. Such a situation can be realized in two ways: (case A) the filament is surrounded by a suspension of active or living particles such as synthetic self-propelling colloids or living bacteria,[20–25] or (case B) the filament is itself comprised of tightly and elastically coupled self-propelling monomeric agents.[26] As in the purely thermal non-active (passive) case, delta-correlated random forces are exerted as the bath molecules collide with the filament and deform it. In addition to these forces, however, the filament is subject to athermal random forces due to interactions between the

passive filament and the active particles as in case A or due to the random displacements between connected active particles as in case B. In case B, the active particles comprising the bead can change their orientation direction diffusively at intermediately long time scales independently of their translational motion. A related example in which the activity comes from the ambient is the mixed poroelastic active–passive matrix environment of eukaryotic cells.[5,9–11,27,28] Filaments in such settings can behave as described in case A, except that statistical the properties of the activity and active stochastic forces (due to motor activity rather than free self-propelling bacteria) may be different.[13]

A key question in these problems is how local bending fluctuations, and indeed metrics for the size and shape of the filament as a whole, are related to intrinsic properties such as the coarse-grained effective bending modulus K_b of the filament, its contour length L, the temperature of the ambient medium T, and importantly the *activity*. An equally important question is to understand how these metrics impact the response of the filament to external stretching or compression forces—i.e., the force-extension relationship that encapsulates the coarse-grained elastic response of the filament—in the *presence of activity*. Finally, besides the properties of the filament or the embedding medium is the important role of constraints and boundary conditions in these settings. Filaments often perform mechanical functions and interact with their networked environment through cross-links or have other similar constraints placed on them. Thus, boundary conditions are anticipated to play very important roles by constraining the space of possible configurations that can be attained.

Two powerful models have been traditionally used to study the stochastic deformations of filaments in passive settings—the Freely Jointed Chain (FJC) and the Worm-Like Chain (WLC) models.[10] Of the two, the Worm-Like Chain model (WLC) allows the incorporation of backbone elasticity as well as configurational entropy[1,2,4,5,7,29] and is particularly suited for stiff to semiflexible polymers and biofilaments. This approach has been successful in describing the elastic properties of a variety of biomolecules, such as ssDNA, dsDNA, RNA, and polypeptide chains (a comprehensive summary may be had from Ref. 10 and bibliography therein). Consequently, WLC models and variants appropriate for semi-flexible or stiff passive polymers/filaments have also been extended to active settings;[30,31] specifically, the properties of the filaments and, complementarily, of the environment are determined in one of two ways.

The first approach is to study the fluctuations of freely suspended filaments. The geometrical size and shape of an ensemble of such suspended fluctuating filaments can be quantified by comparing L with effective radius of gyration R_g and a suitably projected end-to-end distance X. Visual inspection of the ensemble of contour shapes provides the effective persistence length ε—the length scale over which parts of the full filament are orientationally correlated. Soft, long filaments such as DNA in water-like fluid at room temperature typically satisfy $\varepsilon \ll L$ and form blob-like compact conformations with $R_g \ll L$. Stiff filaments such as microtubules at room temperature do not adopt blob-like configurations; their end-to-end distance $\sim L$ and $\varepsilon \sim L$. In the absence of activity and at equilibrium, $K_b = \varepsilon k_B T$, where k_B is the Boltzmann constant. When thermal forces dominate elastic forces, as for a long soft blob-like polymer, the end-to-end distance is $\sim \sqrt{L\varepsilon}$; the radius of gyration scales similarly but with a different pre-factor. When activity is present, the relationship between ε and T is modified; bending energies corresponding to different Fourier modes are no longer related to T via the equipartition theorem. Here, activity serves as a source of energy but not as a sink—dissipation is ultimately due to passive viscosity effects. Recent papers on free active filaments or passive filaments in active fluids studied these novel properties in detail.[30,31]

Here, we focus on a second approach that deduces filament properties from a consideration of its quasi-static *stretching response to imposed pulling forces* under suitable chosen constraints. This approach is motivated by dramatic advances in experimental single molecule techniques such as atomic force microscopy (AFM), optical tweezers and optical traps, magnetic tweezers, and pipette based force apparatus that allow stretching forces to be applied directly to the ends. These quasi-static experiments allow us to identify stiffening or softening responses as the polymer stretches by studying local variations of the force-extension curve as a function of extension.

Our starting point (Sec. II) is the Langevin equation mimicking a passive elastic curve bending under the influence of both thermal and active stochastic forces each with experimentally motivated stochastic properties and spatiotemporal correlations. The formalism follows the Gaussian semiflexible polymer model proposed in Eisenstacken *et al.*;[30,31] similar models have been treated and studied elsewhere.[32–34] Active particles in this model move around in the constant temperature fluid with speed V_0 and an effective viscosity dependent rotational drag coefficient γ_R. Note that Eisenstacken *et al.*[30,31] considered unconstrained suspended filaments with free boundary conditions. Here, we introduce the general solutions to the Langevin equations and obtain formal expressions for the mean square deformation and the mean stretch using appropriate eigenfunction expansions, with these being controlled by the boundary conditions and nature of constraints. In Sec. III, we introduce three canonical boundary conditions motivated by experiments. General solutions to the Langevin equation are specialized to each of the three boundary conditions, and analytical (and in some cases, closed form) force-extension relationships and expressions are derived. The expressions for hinged–hinged boundary conditions are reminiscent of the worm-like-chain model and feature effective bending moduli and mode-dependent non-thermodynamic effective temperatures controlled by the imposed force and by the activity. In Sec. IV, we analyze these expressions for realistic parameter values and illustrate how our results provide methods to estimate the activity from experiments. We conclude in Sec. V by motivating future avenues for theoretical and experimental work.

II. ACTIVE POLYMER MODEL

A. Langevin equation for active polymer

We will use the framework of Eisenstacken *et al.*[30,31] in this paper but study the fluctuations of constrained active polymers (see also Refs. 35 and 36) relevant to biophysical and biological boundary conditions that, to the best of our knowledge, have not been studied elsewhere. In contrast to Eisenstacken *et al.*,[30,31] (a) we do not allow (at hydrodynamic time scales) motion of the center of mass of the filaments, so the filaments cannot translate but can explore the full range of bending fluctuations, (b) we work in a constant tension and constant temperature ensemble that allows us to deduce the

TABLE I. List of parameters.

Symbol	Description	Units	Typical values
ℓ	Filament diameter	m	7×10^{-9}
L	Filament length	m	6.82×10^{-5}
T	Temperature	K	300
k_B	Boltzmann constant	N m K^{-1}	1.38×10^{-23}
γ_R	Damping factor	s^{-1}	0.16
γ	Translational friction coefficient	N s m^{-2}	1.47×10^{-3}
F	Applied tension	N	1×10^{-12}
ε	Persistence length	m	1.71×10^{-5}
K_b	εk_BT	N m^2	7×10^{-26}
V_0	Propulsion velocity	m s^{-1}	$5–25 \times 10^{-6}$
Γ	Stochasticity	N m^{-1}	6.09×10^{-24}

force-extension relations for the filaments immersed in active baths, and (c) we consider several boundary conditions that are applicable to different types of single molecule experiments. For example, the cantilever boundary condition considered in this paper can be applied to tethered particle experiments on filaments in active baths as a method to quantify the activity of the particles via deduction of V_0 from routine measurements of bead fluctuations. In these constrained settings, we expect activity to further enhance differences between the WLC passive model and the active polymer model with non-thermal active fluctuations sometimes controlling filament configurations. Changes in the filament's local curvature and curvature distributions are coupled to local injection and dissipation of energy by the actions of the active agents.

We start with the Gaussian semiflexible polymer model (or a fluctuating rod/filament model or an elastic line model)[30,31] in which the polymer shape is completely defined by the locus of Lagrangian points coincident with the backbone at every time instant t. This, in turn, is treated as a continuous vector (curve) $\mathbf{r}(t, s)$, continuously differentiable, and parameterized by the arc–length parameter s with $-L/2 < s < L/2$. The evolution of $\mathbf{r}(t, s)$ is governed by a Langevin equation and has been derived earlier,[29]

$$\frac{\partial}{\partial t}\mathbf{r}(s,t) = \left(\mathbf{v}(s,t) + \frac{1}{\gamma}\mathbf{\Gamma}(s,t)\right) + \left[\frac{F}{\gamma}\frac{\partial^2}{\partial s^2}\mathbf{r}(s,t) - \varepsilon\frac{k_B T}{\gamma}\frac{\partial^4}{\partial s^4}\mathbf{r}(s,t)\right]. \tag{1}$$

The meaning for each parameter in this equation is given in Table I. Note that terms within parenthesis on the right are stochastic terms, while the ones within the square bracket represent deterministic linear terms. In particular, F is the externally applied force assumed to be along the $\mathbf{e}_1$ direction in the lab frame. The decomposition $\mathbf{r}(s, t) = x(s)\mathbf{e}_1 + y(s)\mathbf{e}_2$ provides components in two directions $\mathbf{e}_1$ and $\mathbf{e}_2$. Let $\theta(s)$ be the angle between the tangent vector $\mathbf{T}(t, s)$ and the $\mathbf{e}_1$ direction (see Fig. 1). The infinitesimal element along the filament $d\mathbf{r}(s, t) = ds\mathbf{T}(s, t)$ and this element when projected along the two orthogonal axes provide the expressions $\partial x = \partial s \cos\theta$ and $\partial y = \partial s \sin\theta$. Similar to the worm-like-chain model, F is assumed to be large so that the deflections of the filament in the y direction are small enough that the angle in $\sin\theta = \partial y/\partial s$ can be approximated as $\sin\theta \approx \theta$ and $\partial x/\partial s = \cos\theta \approx 1 - \theta^2/2$. This provides a good approximation when $-\pi/6 \le \theta \le \pi/6$ is satisfied such as when F is large or when K_b is large for small F. The condition is also satisfied when the contour length L is smaller than the thermal persistence length. Furthermore, boundary conditions can also play a role as clamped–clamped filaments deflect less than clamped-free (or

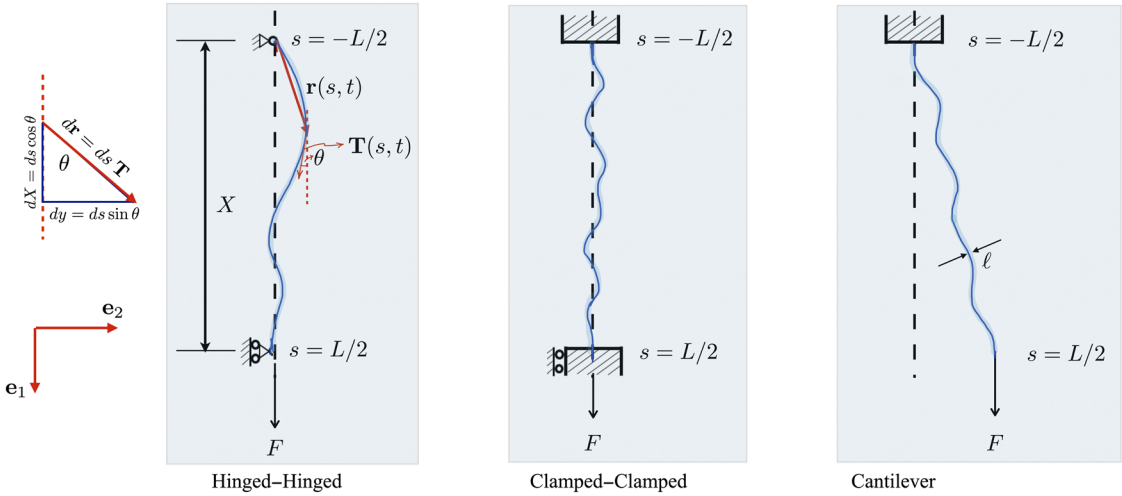

FIG. 1. Schematic figures illustrating the three types of boundary conditions analyzed in this paper. In these scenarios, the active filament or polymer (blue curve) is immersed in a viscous medium. A force F is applied as shown in each case that causes the filament to stretch and orient in the direction of the force. The left-most tile shows projections along and orthogonal to the applied force F.

cantilever) filaments as seen in previous studies by one of us (Purohit *et al.*[37] and Su and Purohit[38]).

In an ensemble where the end-to-end distance X is prescribed, F plays the role of a Lagrange multiplier and enforces the global constraint $X = \int_{-L/2}^{L/2} \cos\theta \, ds$. Here, we operate in an ensemble in which the force F is prescribed and the end-to-end projected distance X will be computed.

Equation (1) exhibits the effects of two random processes—one thermal and one athermal (active). Following Refs. 30 and 31, the term $\mathbf{\Gamma}(s, t)$ is a thermal component that arises from a stochastic Markovian, stationary, and Gaussian process. This fluctuating force has zero mean, and its second moments are given by

$$\langle \Gamma_\alpha(s,t)\Gamma_\beta(s',t')\rangle = 2\gamma k_B \mathrm{T}\delta_{\alpha\beta}\delta(s-s')\delta(t-t'), \tag{2}$$

where T is temperature, k_B is the Boltzmann constant, and γ is the translational friction coefficient per unit length. The influence of athermal noise originating in activity is captured by the velocity term $\mathbf{v}$(s, t). This velocity is a non-Markovian but Gaussian stochastic process with zero mean and the correlation function,[39]

$$\langle \mathbf{v}(s,t)\cdot\mathbf{v}(s',t')\rangle = V_0^2 \ell \exp(-\gamma_R|t-t'|)\delta(s-s'). \tag{3}$$

In reference to case A, the velocity term is an approximation to the manner in which the active agents in the medium interact with the flexible passive filament (see also Ref. 40 for the derivation of this equation). The ratio L/ℓ can in this case be interpreted[30,31] as the number of uniformly distributed active sites along the polymer or equivalently as the number of possible sites active agents in the bath that can access and influence along the polymeric backbone. In reference to case B, V_0 is the self-propulsion speed of the active agent, $\gamma_R \sim D_R$ is its rotational diffusivity, and ℓ may be thought of as a characteristic thickness of the active agent.

We conclude this section by noting that Eq. (1) and subsequent analysis can also be used to analyze active motor-driven fluctuations of filaments. This is readily done by replacing the first term on the right involving the active velocity with a motor active force density using $\mathbf{v} = \mathbf{F}^m/\gamma$. A simple approximation can be derived when motors acting along the filament are assumed to be in one of two states—either attached (on) or detached (off)—with attachment and detachment frequencies ω_{on} and ω_{off}, respectively. The active force per motor f_m^0 depends on the friction coefficient γ characterizing the ambient fluid properties as here, the duty ratio of the motor, and details of the active force generating mechanisms. The active force density due to motors is then $f_a \sim \rho_m f_m^0 \omega_{on}(\omega_{on}+\omega_{off})^{-1}$, with ρ_m being the line density of motors along the filament. Following previous studies,[13] we write

$$\langle F_\alpha^m(s,t)F_\beta^m(s',t')\rangle = \mathscr{M}^2 \ell\, \delta_{\alpha\beta}\exp(-\gamma_R|t-t'|)\delta(s-s'), \tag{4}$$

where $\mathscr{M}^2 \sim (\omega_{off}/\omega_{on})f_a^2$ reflects the effective strength of the motor activity. Here, γ_R is to be interpreted as the inverse of an average time scale for motor activity felt by the microtubule, $\gamma_R = (\omega_{on} + \omega_{off})$. With this mapping done, we go back to the form presented in Eqs. (1)–(3) for analysis as below; however, the results presented in Secs. II D, II E, and III can be extended in a straightforward manner to scenarios where Eqs. (1), (2), and (4) are appropriate.

B. WLC predictions for stretched passive polymers

Before we analyze the Langevin equation for the active filament/polymer further, we first summarize previous results obtained from WLC models for semi-stiff polymers in the absence of activity. For long WLC polymers of length L in thermal equilibrium, the persistence length ε and the mean square end-to-end distance are given by

$$\langle R^2\rangle = 2L\varepsilon - 2\varepsilon^2\left[1-\exp\left(-\frac{L}{\varepsilon}\right)\right]. \tag{5}$$

When such a polymer is stretched by applying tensile forces of magnitude F at the ends, the asymptotic expression for average end-to-end distance in the large force limit is $\langle X\rangle \approx L\left(1-\sqrt{k_B\mathrm{T}/16F\varepsilon}\right)$. More generally, for short polymers or stiff polymers under tension and for large forces,

$$\frac{\langle X\rangle_{\mathrm{WLC}}}{L} \approx \left[1-\frac{1}{4}\sqrt{\frac{k_B\mathrm{T}}{F\varepsilon}}\coth\left(\frac{L}{\varepsilon}\sqrt{\frac{F\varepsilon}{k_B T}}\right)+\frac{1}{4}\frac{\varepsilon}{L}\left(\frac{k_B\mathrm{T}}{F\varepsilon}\right)\right] \tag{6}$$

provides an experimentally usable form of the force-extension relationship.[37] For arbitrary cases, the more accurate form[12]

$$\frac{\langle X\rangle_{\mathrm{WLC}}}{L} = \int_0^1 dz\, \exp\left[\frac{\cosh\left(z\frac{L}{\varepsilon}\sqrt{\frac{F\varepsilon}{k_B\mathrm{T}}}\right)-\cosh\left(\frac{L}{\varepsilon}\sqrt{\frac{F\varepsilon}{k_B\mathrm{T}}}\right)}{4\sqrt{F\varepsilon/k_B\mathrm{T}}\sinh\left(\frac{L}{\varepsilon}\sqrt{\frac{F\varepsilon}{k_B\mathrm{T}}}\right)}\right] \tag{7}$$

has been used. As a point of comparison, we consider the force-extension relationship in a purely entropic framework using the FJC model. Let the FJC polymer of length L be comprised of N straight rigid freely jointed (Kuhn) segments each of size ε. The mean projected length of the polymer when held fixed at one end and stretched by a force F at the other is

$$\frac{\langle X\rangle_{\mathrm{FJC}}}{L} = \coth\left(\frac{\varepsilon F}{k_B\mathrm{T}}\right)-\frac{k_B\mathrm{T}}{\varepsilon F}. \tag{8}$$

Equations (5)–(8) prominently feature the ratio of two energy scales, the force derived scale $F\ell_c$ and the thermal scale k_BT. For the WLC model, the relevant length scale is $\ell_c = \varepsilon$. These expressions serve as a starting point to next look at the effects of activity.

C. Scaled parameters quantifying activity and elasticity

Based on Eqs. (1)–(3), we now introduce important dimensionless parameters that play a role in subsequent analysis.

We first consider activity independent quantities. Three independent aspects need to be taken into account here—the geometry of the filament, the elasticity of the filament based on persistence lengths at the thermodynamic temperature T, and the effect of the imposed force F. The dimensionless parameter is $\mathscr{L}_1 \equiv L/\varepsilon$, with $\varepsilon \equiv K_b/(k_B\mathrm{T})$ being the thermal persistence length the quantifies the effective stiffness at temperature T. When $L \gg \varepsilon$, the filament in the absence of activity behaves as a Gaussian chain. A second dimensionless quantity is $\mathscr{L}_2 \equiv L/\ell_f$, where the length scale for the persistence of force is $\ell_f \equiv \sqrt{\varepsilon k_B\mathrm{T}/F}$. This length-scale determines the distance over which lateral loading or a localized imposed force F creates a deformation. As F increases, ℓ_f decreases, and for

fixed L, the dimensionless parameter $\mathscr{L}_2$ increases, indicating that the filament is increasingly oriented with the direction of F.

It is also useful to define a dimensionless force

$$\mathscr{F} \equiv \frac{F\varepsilon}{k_{\mathrm{B}}\mathrm{T}} \equiv \left(\frac{\varepsilon}{\ell_{\mathrm{f}}}\right)^2 \equiv \left(\frac{\mathscr{L}_2}{\mathscr{L}_1}\right)^2. \tag{9}$$

When $\mathscr{F} \gg 1$, the polymer backbone is stretched predominantly along the direction of the force, and thus, the local tangent angle measured with respect to the direction of F is nearly zero all along the filament. Note that $F \to 0$ with geometric and material properties fixed implies $L/\ell_{\mathrm{f}} \to 0$ and $\mathscr{F} \to 0$. Setting $K_b \to \infty$ implies $\ell_{\mathrm{f}} \to \infty$ and $L/\ell_{\mathrm{f}} \to 0$.

Finally, we introduce parameters that incorporate the characteristics of the active agents. A third dimensionless scale, $\mathscr{L}_3 \equiv L/\ell$, may be defined that provides an estimate for the number density of activity agents or sites. Additionally arising from the self-propelling nature and persistence times associated with the active agents [Eqs. (2) and (3)] and matching previous studies, we define a Peclet number[30,31]

$$\mathscr{P}\mathrm{e} \equiv \frac{\gamma V_0 \ell^2}{k_{\mathrm{B}}\mathrm{T}}. \tag{10}$$

For unconstrained filaments, $\mathscr{P}\mathrm{e}$ is important since the center of mass of the active filament can move, and given the linearity of Eq. (1), we expect terms of the first power in V_0 to control this motion. For constrained filaments, fluctuations in orientation will be important, and this suggests that a different activity parameter will characterize the dynamics.

D. Eigenfunction expansions deliver general expressions for mean square displacements and mean stretch

Following Eisentstacken *et al.*,[30,31] we assume that $\mathbf{r}(s, t)$ has an eigenfunction expansion given below, where $\varphi(s)$ are the orthonormal eigenfunctions of the deterministic and linear part of the stochastic differential equation. Filaments can generally move in a plane or in 3D. Here, we consider the planar motion of the filament and decompose the position vector in terms of orthonormal basis functions

$$\mathbf{r}(s,t) = \sum_{n=0}^{\infty} \boldsymbol{\chi}_n(t)\varphi_n(s), \tag{11}$$

which yields the equation for the projection $y(s, t)$

$$y(s,t) = \mathbf{r}(s,t)\cdot\mathbf{e}_2 = \sum_{n=0}^{\infty} \boldsymbol{\chi}_n(t)\cdot\mathbf{e}_2\,\varphi_n(s) \tag{12}$$

with the associated orthonormality condition on the eigenfunctions $\varphi_n(s)$,

$$1 = \int_{-L/2}^{L/2} \varphi_n^2(s)\,ds. \tag{13}$$

Substituting Eq. (11) in Eq. (1), taking projections, and making use of the orthogonality of the eigenfunctions, we find that $\varphi_n(s)$ satisfies

$$\varepsilon k_{\mathrm{B}}\mathrm{T}\frac{d^4}{ds^4}\varphi_n(s) - F\frac{d^2}{ds^2}\varphi_n(s) = \xi_n\varphi_n(s). \tag{14}$$

The general solution of Eq. (14) is given by

$$\varphi_n(s) = c_{1n}e^{\zeta'_n s} + c_{2n}e^{-\zeta'_n s} + c_{3n}\cos\zeta_n s + c_{4n}\sin\zeta_n s, \tag{15}$$

where

$$\zeta_n = \sqrt{-\frac{1}{2\ell_{\mathrm{f}}^2} + \sqrt{\frac{1}{4\ell_{\mathrm{f}}^4} + \frac{\xi_n}{\varepsilon k_{\mathrm{B}}\mathrm{T}}}}, \quad \zeta'_n = \sqrt{\zeta_n^2 + \frac{1}{\ell_{\mathrm{f}}^2}}. \tag{16}$$

The mode amplitudes in Eq. (12) are related to the stochastic forcing, which are the origin of time dependence.[41] Following the original derivation[30,31] and motivated by the linearity of Eq. (1), we look for stationary functions by decomposing the fluctuating stochastic terms in Eq. (1) in terms of the same eigenfunctions as in Eq. (12). Thus, we write

$$\boldsymbol{\Gamma}(s,t) = \sum_{n=0}^{\infty} \boldsymbol{\Gamma}_n(t)\varphi_n(s), \tag{17}$$

$$\mathbf{v}(s,t) = \sum_{n=0}^{\infty} \mathbf{v}_n(t)\varphi_n(s). \tag{18}$$

Substituting Eqs. (17) and (12) into Eq. (1), we reproduce the primary result from[30,31]

$$\frac{d}{dt}\boldsymbol{\chi}_n = -\frac{1}{\tau_n}\boldsymbol{\chi}_n + \mathbf{v}_n + \frac{1}{\gamma}\boldsymbol{\Gamma}_n(t) \tag{19}$$

with

$$\tau_n = \frac{\gamma}{\xi_n} = \frac{\gamma}{k_{\mathrm{B}}\mathrm{T}\varepsilon\zeta_n^4 + F\zeta_n^2} = \frac{\gamma}{k_{\mathrm{B}}\mathrm{T}\varepsilon}\left(\frac{\ell_{\mathrm{f}}^2}{\ell_{\mathrm{f}}^2\zeta_n^4 + \zeta_n^2}\right). \tag{20}$$

To further proceed and calculate properties such as the end-to-end stretch, we need analytical results for the mode amplitudes. This has been derived earlier in Ref. 30, and we report them here for completeness. The solution and associated orthogonality conditions are

$$\boldsymbol{\chi}_n(t) = e^{-t/\tau_n}\int_{-\infty}^{t} e^{t'/\tau_n}\left(\mathbf{v}_n(t') + \frac{1}{\gamma}\boldsymbol{\Gamma}_n(t')\right)dt', \tag{21}$$

$$\langle\boldsymbol{\chi}_n(t)\cdot\boldsymbol{\chi}_m(t')\rangle = \delta_{mn}\langle\boldsymbol{\chi}_n(t)\cdot\boldsymbol{\chi}_n(t')\rangle. \tag{22}$$

Time correlations have been calculated elsewhere [see Eq. (23) in Ref. 31]. In Eq. (22), δ_{mn} is the Kronecker delta function. In the rest of this paper, we will confine attention of the component of $\mathbf{r}(t, s)$ along the $\mathbf{e}_2$ direction; thus, we will only be interested in the $\mathbf{e}_2$ component of $\boldsymbol{\chi}_n$. This component will be denoted by the scalar χ_n. From complete expressions in Ref. 31, we derive

$$\left\langle(\chi_n(t) - \chi_n(0))^2\right\rangle = \frac{2k_{\mathrm{B}}\mathrm{T}\tau_n}{\gamma}(1 - e^{-t/\tau_n}) + \frac{2V_0^2\ell\tau_n^2}{1+\gamma_R\tau_n}\left(1 - \frac{e^{-\gamma_R t} - \gamma_R\tau_n e^{-t/\tau_n}}{1-\gamma_R\tau_n}\right). \tag{23}$$

Statistically stationary properties are obtained in the limit where the memory of initial conditions is lost; thus, taking the limit $t \to \infty$ in Eq. (21), we can calculate ensemble averaged correlation functions in the long time limit. Further insight may be had by examining in certain limits. The small time expansion of Eq. (23) confirms that

$$\left\langle(\chi_n(t) - \chi_n(0))^2\right\rangle \sim \frac{2k_{\mathrm{B}}\mathrm{T}t}{\gamma}, \quad t \ll \max(\tau_n, \gamma_R^{-1}) \tag{24}$$

and independent of F. We note that τ_n depends on F via Eq. (20). When $t \gg \max(\tau_n, \gamma_R^{-1})$,

$$\left\langle (\chi_n(t) - \chi_n(0))^2 \right\rangle \sim \frac{2k_B T \tau_n}{\gamma}\left(1 + \frac{V_0^2 \ell \gamma}{k_B T \gamma_R}\frac{\gamma_R}{\tau_n(1+\gamma_R\tau_n)}\right) \quad (25)$$

and thus is strongly dependent on both F and V_0.

E. Expressions for the mean square displacement

Eisenstacken *et al.*[30,31] considered free filaments that are allowed to diffuse and therefore have a non-zero mean square displacement (stationary state value), that is, $\langle \Delta \mathbf{r}_{cm}^2 \rangle$ is, in general, non-zero. Here, we consider constrained filaments that are prevented from global translation and therefore ignore this term.

The mean square value of the y displacement $y(s, t)$ with $-L/2 \le s \le L/2$ at steady state can be obtained by taking the statistically stationary average as $t \to \infty$ of Eq. (23), which gives

$$\begin{aligned}\left\langle y^2(s) \right\rangle &= \lim_{t\to\infty} \sum_{n=1}^{\infty} \varphi_n^2(s) \left\langle (\chi_n(t) - \chi_n(0))^2 \right\rangle \\ &= \sum_{n=1}^{\infty} \varphi_n^2(s) \left[\frac{2k_B T \tau_n}{\gamma} + \frac{2V_0^2 \ell \tau_n^2}{1+\gamma_R \tau_n} \right], \end{aligned} \quad (26)$$

where Eq. (23) has been used in going from the first to the second expression on the right-hand side. We note that activity enters through the eigenfunction as well as the multiplying factor in square brackets while, the tension ~F enters explicitly through the eigenfunction.

Note that the two terms in the square bracket in Eq. (26) provide information about two complementary features of the activity. The first term gives an indication of the time scale over which correlations due to thermal noise decay (via τ_n), and this incorporates the effect of F [see Eq. (20)] but does not contain the influence of activity. The second term on the other hand explicitly incorporates the effect of active self-propulsion from its dependence on V_0 and also the geometry of the agents through ℓ.

F. Expressions for the mean stretch

Apart from the mean square displacement, we are also interested in the force-extension relation. We use X to denote the projected length of the filaments onto the x axis (see Fig. 1) so that $dX/ds = \cos\theta(s, t)$, where $\theta(s)$ is the angle between the unit tangent vector $d\mathbf{r}/ds$ at point s and the $\mathbf{e}_1$-axis. We assume that the displacements are small and $\sin\theta \approx \theta$ so that

$$\frac{dy}{ds} = \sin\theta(s,t) \approx \theta(s,t) = \sum_n \chi_n(t)\varphi_n'(s). \quad (27)$$

Next, using $\cos\theta \approx 1 - \theta^2/2$, we obtain

$$\begin{aligned}\frac{\langle X \rangle}{L} &= \frac{1}{L}\left\langle \int_{-\frac{L}{2}}^{\frac{L}{2}} \cos\theta ds \right\rangle \approx \frac{1}{L}\left\langle \int_{-\frac{L}{2}}^{\frac{L}{2}} \left(1 - \frac{\theta^2}{2}\right) ds \right\rangle \\ &= 1 - \frac{1}{L}\left\langle \int_{-\frac{L}{2}}^{\frac{L}{2}} \frac{\theta^2}{2} ds \right\rangle, \end{aligned} \quad (28)$$

which evaluates to

$$\frac{\langle X \rangle}{L} = 1 - \frac{1}{L}\int_{-\frac{L}{2}}^{\frac{L}{2}} \sum_{n=1}^{\infty} \left[\frac{2k_B T \tau_n}{\gamma} + \frac{2V_0^2 \ell \tau_n^2}{1+\gamma_R\tau_n} \right] \frac{\varphi_n'(s)^2}{2} ds. \quad (29)$$

III. RESULTS: ANALYSIS OF CONSTRAINED ACTIVE FILAMENTS

Here, we begin with the general forms of the equations in Secs. II D–II F for the eigenfunctions given by Eqs. (14)–(16), equations for the mode amplitudes given by Eqs. (17)–(21), and the analytical expressions Eqs. (26) and (29). Specific forms for the eigenfunctions are determined for different boundary conditions, and from these, reduced expressions for Eqs. (26) and (29) for the case at hand are derived and analyzed.

A. Hinged–hinged boundary condition

Under hinged–hinged boundary conditions, the moments at the ends of the filament are zero, and this is usually modeled in mechanics by hinges that allow free rotation, as illustrated in Fig. 1. The boundary constraint is therefore soft in that the hinges resist forces and prevent translation degrees of freedom but allow for free rotation. The active filament is subject to an applied tension acting in the x-direction at one end as in the figure. The hinge is at the end where the force is applied is on a roller so that it can move in the x-direction to change the end-to-end distance or effective extension of the filament.

Note that the hinged ends can support forces. Specifically, the roller does not allow motion in the y-direction (perpendicular to the tension); hence, there is a reaction (shear) force at the end. This reaction force does not enter the potential energy of the filament since it does not do work. Experimentally, the hinged–hinged boundary condition may be realized by using an optical trap (which allows free rotation) to pull one end of the filament, while the other end is held in a second optical trap or is immobilized by some other means.

The appropriate boundary conditions that need to be imposed on Eq. (12) in this case correspond to the constraints of no displacement and zero moment. The curvature is $\kappa = |d^2\mathbf{r}/ds^2|$, which can be approximated by $\kappa = \partial^2 y/\partial s^2$ for small y. Assuming that the moment is proportional to κ as in classical Kirchhoff–Love rod theory, the boundary conditions can be written as

$$y\left(\pm\frac{L}{2}, t\right) = 0, \quad y''\left(\pm\frac{L}{2}, t\right) = 0, \quad (30)$$

where $'$ denotes differentiation with respect to s. Substituting Eq. (30) into Eq. (15) and imposing that the s dependence of $y(t, s)$ arises only from $\varphi(s)$ in the eigenfunction expansion Eq. (12), we obtain the eigenvalues and eigenfunctions

$$\zeta_n = \frac{n\pi}{L}, \quad n \in \mathbb{N}_0, \quad (31)$$

$$\varphi_n(s) = \sqrt{\frac{2}{L}} \sin\left(\frac{n\pi s}{L} + \frac{n\pi}{2}\right). \quad (32)$$

Thus, the eigenvalues and eigenfunctions take a particularly simple form that is amenable to analysis using Fourier series. With these, we can now evaluate statistical properties of this constrained elastic filament. In Secs. III A 1 and III A 2, we will combine Eqs. (31) and (32) with Eqs. (26) and (29) valid in the statistically relevant $t \to \infty$ limit to derive expressions, in some cases closed form and analytical, for the mean square displacement and the mean extension (mean stretch) of the active polymer.

1. Mean square displacement

Equation (26) can be rewritten [Eqs. (B1)–(B8)] as

$$\langle y^2(s)\rangle = \sum_{n=1}^{\infty}\frac{2}{L}\sin^2\left(\frac{n\pi s}{L}+\frac{n\pi}{2}\right)\left[\frac{2k_{\mathrm{B}}\mathrm{T}\tau_n}{\gamma}+\frac{2V_0^2\ell\tau_n^2}{1+\gamma_R\tau_n}\right]$$

$$\langle y^2(s)\rangle = \sum_{n=1}^{\infty}\frac{2}{L}\sin^2\left(\frac{n\pi s}{L}+\frac{n\pi}{2}\right)\frac{2k_{\mathrm{B}}\mathrm{T}\tau_n}{\gamma} + \sum_{n=1}^{\infty}\frac{2}{L}\left(\frac{1}{2}-\frac{1}{2}\cos\left(\frac{2n\pi s}{L}\right)(-1)^n\right)\frac{2V_0^2\ell\tau_n^2}{1+\gamma_R\tau_n}. \quad (33)$$

To ease the analysis, we further introduce intermediate variables

$$a \equiv \frac{k_{\mathrm{B}}\mathrm{T}\varepsilon\pi^4}{L^4}, \quad b \equiv \frac{F}{L^2}\pi^2, \quad c = 2V_0^2\ell\gamma^2, \quad d \equiv \gamma_R\gamma, \quad (34)$$

and

$$r_1 = \frac{b-\sqrt{b^2-4ad}}{2a}, \quad r_2 = \frac{b+\sqrt{b^2-4ad}}{2a}. \quad (35)$$

Simplifying Eq. (33) further [see Eqs. (B9)–(B13)] and using Eqs. (34) and (35) to rewrite the results, we obtain an analytical expression for the mean square displacement valid for the hinged–hinged boundary conditions [Eq. (A1), see Appendix A], from which the simplified asymptotic expansion valid for large F [Eq. (36)] is obtained as follows:

$$\langle y^2(s)\rangle(F\to\infty) \sim -\frac{\pi V_0^2\ell\gamma^2}{L}\left[\frac{\mathrm{csch}(\pi\sqrt{r_1})(\cosh(\pi\sqrt{r_1})-\cosh(2\pi\sqrt{r_1}s/L))}{ar_1^{3/2}\sqrt{b^2-4ad}(b/a-r_1)}\right] + \frac{\varepsilon L}{2\mathscr{F}}\left(1-\frac{4s^2}{L^2}\right)\left(1+\frac{4}{3}\mathscr{A}\right). \quad (36)$$

The last term of Eq. (36) introduces a new dimensionless quantity $\mathscr{A}$,

$$\mathscr{A} \equiv \left(\frac{3V_0^2\ell\gamma}{4k_{\mathrm{B}}\mathrm{T}\gamma_R}\right) \equiv \frac{3}{4}\left(V_0^2/\gamma_R\right)\left(k_{\mathrm{B}}\mathrm{T}/\ell\gamma\right) \quad (37)$$

that can be interpreted as the ratio of two diffusivities, an effective thermal diffusivity based on the hydrodynamic temperature of the solvent or ambient suspending fluid $k_{\mathrm{B}}\mathrm{T}/\ell\gamma$ and an active diffusivity V_0^2/γ_R.[23,42] We note that if the active filament comprised of individual connected active beads (agents) that were deconstructed, each of these self-propelling agents moving by themselves would display long time diffusive behavior with an active component that is $O(V_0^2/\gamma_R)$.

2. Force-extension relation

The force-extension relation for a hinged–hinged filament in an active bath can be derived from Eq. (29) in combination with (31) and (32).

We start with the equation for the statistically averaged mean stretch that is first written as an infinite series in n as in Eq. (33) and then manipulated using steps similar to that described above. We note that the Langevin equation is linear in the activity (specifically in V_0^2). Algebraic manipulations allow us to go from Eq. (33) to the analytical expression

$$\frac{\langle X\rangle}{L} = 1-\frac{1}{L}\int_{-L/2}^{L/2}\sum_{n=1}^{\infty}\frac{2}{L}\frac{\cos^2(n\pi s/L)}{2}\frac{n^2\pi^2}{L^2} \times\left(2\left(\frac{\varepsilon n^4\pi^4}{L^4}+\frac{Fn^2\pi^2}{kTL^2}\right)^{-1}+\frac{2V_0^2\ell\tau_n^2}{1+\gamma_R\tau_n}\right). \quad (38)$$

Equation (38) may then be further simplified to get a closed form (but complicated) expression presented in Appendix A. The terms within the square brackets on the right-hand side in Eq. (A2) are independent of activity; other terms on the right-hand side depend on c linearly.

As $\mathscr{F}\to\infty$, we can ignore $o(\sqrt{1/\mathscr{F}})$ in Eq. (A2) and simplify further to obtain the mean stretch for large force F and arbitrary values of V_0^2 (arbitrary values of c),

$$\frac{\langle X\rangle}{L} = 1-\frac{1}{\sqrt{4K_bF}}\left(k_{\mathrm{B}}\mathrm{T}+\frac{3V_0^2\ell\gamma}{4\gamma_R}\right). \quad (39)$$

Equation (39) demonstrates that (a) the worm-like chain formula can be recovered from Eq. (39) when $V_0 = 0$, which is as expected, and (b) as far as the mean stretch is concerned, in the large F limit, the filament behaves as if it is suspended in a continuous medium with an enhanced higher temperature given by

$$\mathrm{T}\left(1+\frac{3V_0^2\ell\gamma}{4k_{\mathrm{B}}\gamma_R T}\right) = \mathrm{T}(1+\mathscr{A}). \quad (40)$$

B. Modes fluctuate at *effective* higher temperatures

Several studies on the thermodynamics of active suspensions have introduced the concept of an *effective temperature* that takes into account the enhanced effect of activity induced fluctuations. For instance, we have recently studied[23,25] if such a quantity can be defined in a dilute bacterial suspension of *Escherichia coli*[24] by studying the diffusivity of small tracer particles and their speed distribution functions. We found that while useful in interpreting the enhancement in tracer diffusivity, the temperature is not a thermodynamic quantity.[23,25] Effective temperature concepts have been used to study various aspects of active biological matter such as red-blood-cell membrane fluctuations[28] and active matter in general,[23,28,43] among others (cf. discussion in Ref. 25). The equipartition theorem applied to the passive fluid interface and active bacterial interface fluctuations, which like deformation modes in this study store energy,[44–46] similarly provides a relationship between deformation modes and the thermodynamic temperature of the system. This has been used to relate properties such as surface tension and surface energy to the temperature.

Brangwynne *et al.*[27] analyzed the fluctuations of a microtubule that is embedded in a network of actin filaments. When no myosin motors are put into the actin gel, then the microtubule suffers purely thermal fluctuations, as seen in Fig. 2A of their paper. When myosin motors and ATP (adenosine triposphate) are added into the mix, then the microtubule is in an active environment and so the amplitude of its fluctuations increases, as seen in Fig. 2C of their paper. Here, we use the eigenvalues and eigenmodes that we have calculated in Sec. III to see if one can interpret the fluctuations seen in their

experiments (Fig. 2C in their paper) as due to an enhanced effective temperature.

To proceed in our analysis, we revisit Eq. (26) for transverse fluctuations of the active filament given by Eqs. (1)–(3), describing statistics of the random stochastic terms. Let $y^2(s)$ denote

$$\Delta y^2(s) = \lim_{t\to\infty}\left\langle (y(s,t) - y(s,0))^2 \right\rangle$$

where without loss of generality, we assume that information about the initial shape is lost eventually. Noting that τ_n is independent of activity, we rewrite Eq. (26) as follows:

$$\left\langle y^2(s)\right\rangle = \sum_{n=1}^{\infty} \varphi_n^2(s)\left(\frac{2k_{\mathrm{B}}(\mathrm{T}_{\mathrm{eff}})_n\tau_n}{\gamma}\right), \tag{41}$$

$$(\mathrm{T}_{\mathrm{eff}})_n = \mathrm{T} + \frac{V_0^2\ell\tau_n\gamma}{k_{\mathrm{B}}(1+\gamma_R\tau_n)}, \tag{42}$$

where we have introduced a mode-dependent *effective temperature* $(\mathrm{T}_{\mathrm{eff}})_n$ that differs from the thermal temperature (of the solvent) T when $V_0^2 > 0$. Equation (42) indicates that each mode n differs in dynamics through the factor ζ_n. The actual form of the effective temperature will depend on the force exerted; this is due to the presence of τ_n in the activity term—the second term on the right-hand side of Eq. (42).

From the caption of Fig. 2 in Ref. 27, we find that $L = 30$ mm and from the text that $\varepsilon = K_b/k_{\mathrm{B}}\mathrm{T} = 1$ mm and thus $\mathscr{L}_1 \equiv L/\varepsilon \gg 1$; in this limit and for negligible deterministic forces acting along the filament (as in their problem), the boundary condition does not matter in the computation of the amplitudes of the normal modes. Consideration of the basis functions used in their paper suggests that being torque free, the microtubule ends are free to rotate, and hence, a hinged–hinged condition is appropriate. Being consistent with their expression and using Eqs. (31) and (32) in Eq. (41), we get equations for the tangent angle and the curvature $\mathscr{C} = \partial\theta/\partial s'$,

$$\theta(s',t) = \sqrt{\frac{2}{L}}\sum_{n=1}^{\infty}\left(\frac{n\pi}{L}\right)\chi_n(t)\cos\left(n\pi\frac{s'}{L}\right), \tag{43}$$

$$-\mathscr{C}(s',t) = \sqrt{\frac{2}{L}}\sum_{n=1}^{\infty}\left(\frac{n\pi}{L}\right)^2\chi_n(t)\sin\left(n\pi\frac{s'}{L}\right), \tag{44}$$

where we have transformed from used $s'/L = s/L + 1/2$ to transform from our range $s \in (-L/2, L/2)$ to their $s' \in (0, L)$. Choosing the base preferred curvature to be zero, the ensemble averaged bending energy for $F = 0$ is

$$\langle E\rangle = \frac{1}{2}\int_0^L K_b\mathscr{C}^2\,ds' = \sum_{n=1}^{\infty}\frac{K_b}{2}\langle\chi_n^2\rangle\left(\frac{n\pi}{L}\right)^2 = \sum_{n=1}^{\infty}\langle E_n\rangle, \tag{45}$$

where we have exploited orthonormality of basis functions.

In the *absence of activity*, equipartition holds, and thus, the average energy in each mode of fluctuation per degree of freedom is $\frac{1}{2}k_{\mathrm{B}}\mathrm{T}$. In two dimensions, equating each mode $\langle E_n\rangle$ to $k_{\mathrm{B}}\mathrm{T}$, we obtain

$$\langle\chi_n^2\rangle = \frac{2k_B\mathrm{T}}{K_b\zeta_n^2}, \tag{46}$$

which is the expected result for $V_0 = 0$ and reproduces the result in the work of Brangwynne *et al.*

In the presence of motors, the system is not thermodynamic anymore, and activity causes fluctuation amplitudes to increase relative to the thermal amplitudes. We then ask if an extended formula

$$\langle\chi_n^2\rangle = \frac{2k_B(\mathrm{T}_{\mathrm{eff}})_n}{K_b\zeta_n^2} \tag{47}$$

may be used to interpret experimental measurements of microtubule fluctuations in the presence of motors added. Note that the form of Eq. (42) emphasizes how activity enables this system to break free of some of the constraints imposed by fluctuation dissipation—specifically, activity leads to enhanced amplitudes, especially at small mode numbers ζ_n due to the second term being a function of τ_n. Note that we do not have detailed knowledge about motor activity (such as the motor forces, duty ratios, and attachment probabilities) needed to quantify the parameters in Eq. (4).

Equation (23) indicates that when activity is absent, $\langle\chi_n^2\rangle$ is approached exponentially in time t. Figures 2A and 2C of Brangwynne *et al.*[27] give $\langle\chi_n^2(t)\rangle$ at four different values of t. Choosing $\zeta_n = 0.7$ mm^{-1} and fitting the four values in time from Fig. 2A to a simple decaying exponential

$$\langle\chi^2(t)\rangle = \langle\chi^2\rangle_{\max} - b_0\exp\left(-\frac{t}{\tau}\right), \tag{48}$$

we find $\tau = 3.63$ s and $b_0 = 2.67$ nm consistent with $k_BT \approx 4.1$ pN nm. The data points and the fit are shown in black in Fig. 2.

When activity is present, Eqs. (23) and (24) suggest a trajectory in time that is no longer a simple decaying exponential; indeed setting $F = 0$ in these shows the presence of a constant time independent term and two decaying exponentials with opposite signs. For simplicity, here we, however, retain the form in Eq. (48) and treat $\langle\chi^2\rangle_{\max}$, τ, and b_0 as functions of activity. Choosing the same value of ζ_n, we fit the data extracted in Fig. 2C and obtain $\tau = 3.63$ s, $b_0 = 26$ nm, and $k_B\mathrm{T}_{\mathrm{eff}} \approx 30.5$ pN nm, suggesting a significant activity driven component to the microtubule fluctuations. These points and the fit are plotted in red in Fig. 2. These curves are to be compared

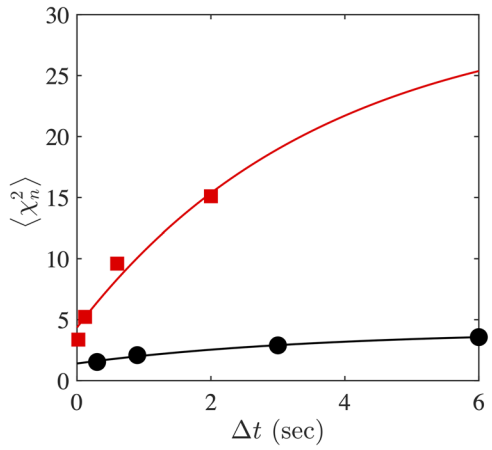

FIG. 2. Black data and line correspond to $q = 0.7$ mm^{-1} from Fig. 2A of Brangwynne *et al.*,[27] and red data and line to $q = 0.7$ mm^{-1} from Fig. 2C of the same paper.

with Fig. 3 of Ref. 27 in which the curve for $\langle \chi_n^2 \rangle$ also flattens out as t becomes large.

C. Clamped–clamped boundary condition

1. Mean square displacement

Clamped–clamped boundary conditions are relevant when no y displacements or rotations are allowed at both ends of the filament. Thus, there are non-zero shear and moment reactions at the two ends, but they do not enter the potential energy of the filament because they do no work. This type of boundary condition is relevant in assays in which filaments (actin or microtubules) bridge a channel (see Arsenault *et al.*[47]) while both their ends are attached to the substrate. This type of assays is often used to study the motion of molecular motors as they walk along the filament (the channel allows the motors to rotate around the filament without hindrance). The filaments can be under tension before being attached to the substrate as Arsenault *et al.*[47] demonstrated by using electric fields in the case of actin filaments. It is not difficult to visualize a single molecule experiment in which a clamped–clamped boundary condition is applied together with a tensile force at one movable (in the x direction) end.

The clamped constraint at each end means that the angle made by the filament with the $\mathbf{e}_1$ axis is fixed. Here, we assume that the clamping keeps the filament perfectly aligned with the direction of the force at $s = \pm L/2$. The boundary conditions for the clamped–clamped filament are

$$y\left(\pm\frac{L}{2},t\right) = 0, \quad y'\left(\pm\frac{L}{2},t\right) = 0. \tag{49}$$

Combining Eqs. (49) and (15) yields the following two sets of solutions (see Appendix B). The first eigenvalue eigenfunction set is

$$-\tan\left(\zeta_n\frac{L}{2}\right) = \tanh\left(\zeta_n'\frac{L}{2}\right)\frac{\zeta_n'}{\zeta_n}, \tag{50}$$

$$\varphi_n(s) = \kappa_{1n}\left[\frac{\cosh\left(\zeta_n' s\right)\zeta_n}{\sinh\left(\zeta_n'\frac{L}{2}\right)} + \frac{\cos\left(\zeta_n s\right)\zeta_n'}{\sin\left(\zeta_n\frac{L}{2}\right)}\right], \tag{51}$$

where ζ_n, ζ_n' can be solved from Eqs. (16) and (50). The second set is given by the two equations

$$\tan\left(\zeta_n\frac{L}{2}\right) = \tanh\left(\zeta_n'\frac{L}{2}\right)\frac{\zeta_n}{\zeta_n'}, \tag{52}$$

$$\varphi_n(s) = \kappa_{2n}\left[\frac{\sinh\left(\zeta_n' s\right)\zeta_n}{\cosh\left(\zeta_n'\frac{L}{2}\right)} - \frac{\sin\left(\zeta_n s\right)\zeta_n'}{\cos\left(\zeta_n\frac{L}{2}\right)}\right]. \tag{53}$$

Here, κ_{1n} and κ_{2n} in Eqs. (51) and (52) are given in Appendix A, Eqs. (A3) and (A4).

Lacking any straightforward algebraic manipulations that can yield a closed form expression as in the hinged–hinged case, we just use the series summation to evaluate the mean square displacement. Using 100 terms in the series proved more than adequate; 10 terms were insufficient, indicating that the series, while converging to the exact value, does so moderately fast:

$$\left\langle y^2(s)\right\rangle = \sum_{n=1}^{100}\varphi_n^2(s)\left[\frac{2k_{\mathrm{B}}\mathrm{T}\tau_n}{\gamma} + \frac{2V_0^2\ell\tau_n^2}{1+\gamma_R\tau_n}\right]. \tag{54}$$

2. Force-extension relation

There is no closed form solution for Eq. (29) under the clamped–clamped boundary condition, so here as well we sum the first $N = 100$ terms of the series to obtain a sufficiently accurate value [here, we use Eqs. (51) and (53) to compute $\varphi_n'(s)$],

$$\frac{\langle X\rangle}{L} \approx 1 - \frac{1}{L}\int_{-\frac{L}{2}}^{\frac{L}{2}}\sum_{n=1}^{100}\left[\frac{2k_{\mathrm{B}}\mathrm{T}\tau_n}{\gamma} + \frac{2V_0^2\ell\tau_n^2}{1+\gamma_R\tau_n}\right]\frac{\varphi_n'(s)^2}{2}ds. \tag{55}$$

D. Cantilever boundary condition

The cantilever boundary condition corresponds to one free end and one clamped end as illustrated in Fig. 1. The free end has zero shear force and moment, while the clamped end has both shear and moment reactions that do no work. This boundary condition is relevant to tethered particle experiments in single molecule mechanics. Often, the deflections of the tethered particle are measured in these experiments to deduce the length of the tether. A tensile force can be exerted on the particle by the use of magnetic tweezers. This tensile force does work through the motion of the bead and thus changes the end-to-end distance of the filament.

Intuitively, given the degree of freedom at the free end and the lack of a spatially localizing constraint there, deformations are expected to be larger compared to the hinged–hinged or clamped–clamped boundary conditions. Still, the force-extension relationship and the mean square displacements may be obtained within the theoretical framework laid out in Sec. III D 2 as described below.

1. Mean square displacement

We next calculate the mean square displacement by first finding the associated eigenvalues and eigenfunctions. The cantilever boundary conditions are

$$y\left(-\frac{L}{2},t\right) = 0, \quad y'\left(-\frac{L}{2},t\right) = 0, \quad y''\left(\frac{L}{2},t\right) = 0,$$

$$K_b y'''\left(\frac{L}{2},t\right) - F y'\left(\frac{L}{2},t\right) = 0. \tag{56}$$

Re-defining $\hat{r}(s') = r(L/2 + s)$, we rewrite the general solution for eigenfunction [Eq. (15)] in the following way:

$$\begin{aligned}\hat{\varphi}_n(s') = {} & t_{1n}\left[\cos\left(\zeta_n s'\right) + \cosh\left(\zeta_n' s'\right)\right] \\ & + t_{2n}\left[\cos\left(\zeta_n s'\right) - \cosh\left(\zeta_n' s'\right)\right] \\ & + t_{3n}\left[\sin\left(\zeta_n s'\right) + \sinh\left(\zeta_n' s'\right)\right] \\ & + t_{4n}\left[\sin\left(\zeta_n s'\right) - \sinh\left(\zeta_n' s'\right)\right].\end{aligned} \tag{57}$$

The first boundary condition $\hat{\varphi}_n(0) = 0$ implies $t_{1n} = 0$. The second boundary condition $\hat{\varphi}_n{}'(0) = 0$ implies

$$t_{3n} = \frac{\zeta_n' - \zeta_n}{\zeta_n' + \zeta_n}t_{4n}. \tag{58}$$

Using Eq. (58), the third boundary condition $\hat{\varphi_n}''(L) = 0$ implies Eq. (A5) (see Appendix A). Imposing the boundary condition $K_b\hat{\varphi_n}'''(L) = F\hat{\varphi_n}'(L)$ [to get Eq. (A6)] and combining Eqs. (58)–(A6), we get Eq. (A7) of Appendix A, where the wave numbers ζ_n and ζ_n' can be solved from Eqs. (16) and (A7). Using $s' = s + \frac{L}{2}$, the eigenfunction can be written down in closed form as

$$\begin{aligned}\varphi_n(s) = t_{2n}\cos\left(\zeta_n\left(s+\frac{L}{2}\right)\right) - t_{2n}\cosh\left(\zeta_n'\left(s+\frac{L}{2}\right)\right)\\ + (t_{3n}+t_{4n})\sin\left(\zeta_n\left(s+\frac{L}{2}\right)\right)\\ + (t_{3n}-t_{4n})\sinh\left(\zeta_n'\left(s+\frac{L}{2}\right)\right),\end{aligned} \tag{59}$$

where the constants t_{2n} and t_{3n} are functions of t_{4n} through Eqs. (A5) and (58). The constant t_{4n} is solved by imposing the constraint $\|\varphi_n(s)\|_{L^2} = 1$ and orthonormalizing the eigenfunctions using Eq. (13). Similarly, we used Eq. (54) to compute $\langle y^2(s)\rangle$.

2. Force-extension relation

Again, there is no closed form solution for Eq. (29) under the cantilever boundary condition, so we use Eq. (55) to approximate the force-extension relation and Eq. (59) as the appropriate eigenfunctions corresponding to the cantilever boundary condition.

IV. DISCUSSION

Here, we analyze the expressions derived earlier and study how active noise modifies statistical properties for biologically realistic values of the tension F. In Sec. III, we started from the evolution of polymer configurations using an *active extension* of the classical Langevin equation that has two stochastic components—the active noise due to the self-propulsion velocity $\mathbf{v}(s, t)$ and the thermal fluctuating drag $\boldsymbol{\Gamma}(s, t)$. We then obtained explicit expressions for statistical stationary state averages for the mean square displacement and for the mean stretch of an active polymer subject to a tension in an ensemble where the temperature T is held constant. Contrary to other related works, the analysis in this section was specifically for tethered not free polymers. Associated deformations and effective force-extension relationships therefore depend crucially on the type of constraint at the boundary.

A. Predictions of theory for weak and strong tension

We choose the tension F applied at $s = L/2$ to have values 0.1 pN, 1 pN, and 10 pN. The appropriate parameter to study in order to elucidate the effects of activity is the dimensionless parameter $\mathscr{A}$. We choose $\mathscr{A} = 0.1$, 1, and 10 spanning low activity, moderate activity, and high activity regimes. Note that since the geometric properties of the filament and the thermal temperature T are held constant, activity variations correspond to changes in the self-propulsion speed V_0.

We compare the mean square displacement for the three types of boundary conditions under these parameters—these are given by Eqs. (30), (49), and (56), respectively. The results are plotted in Figs. 3(a) and 3(b). We see from Fig. 3(a) that $\langle y^2(s)\rangle$ is maximum at $s = 0$, or the center of the filament, for the hinged–hinged and clamped–clamped boundary conditions. For the cantilever boundary condition, $\langle y^2(s)\rangle$ is maximum at the end $s = L/2$ as expected. The mean square displacement is predicted to be the smallest for the clamped–clamped filaments because they are the most constrained.

In Fig. 3(b), we show the variation in the mean square lateral displacements at the central point of the polymer filament as a function of the imposed extensional force F for low, moderate, and high activity ($\mathscr{A} = 0.1, 1.0$, and 10.0, respectively). A closer examination of the figures (not shown) indicates that as F increases to 10 pN and beyond, the hinged–hinged and clamped–clamped results tend to approach each other. This is because the filament is stretched straight under large tension so that the tangent vectors are almost all aligned along the $\mathbf{e}_1$-axis—this happens even when the ends are hinged. For the cantilever boundary condition, we observe significant curvature changes near the $s = L/2$ end in the limit of small imposed tension and large activity. In general, the mean square displacements decrease as applied tension increases and increase as active noise increases. However, the effect of increasing force is more significant than the increasing active noise in the parametric range studied here.

The results depicted in Fig. 3 for small applied tensions ($F = 0.1$ pN) are close to expressions analyzed in Ref. 37 in the absence of activity and serve as a check to confirm (thus validate) that expressions derived here for clamped–clamped and hinged–hinged boundary conditions recover results of Ref. 37 when $V_0 = 0$.

To investigate systematically the effect of the imposed force on the force-extension results, we choose $L/\varepsilon = 4$ and analyze the expressions at three different activity values $\mathscr{A} = 0.1$, 1, and 10. Note that here entropic effects dominate for contour lengths that are long compared to the persistence length. Figure 4 shows our theoretical results; we see that under all magnitudes of activity, the force F needed to attain the same value of $\langle X\rangle/L$ is the highest for the cantilever and the lowest for the clamped–clamped condition. As $\mathscr{A}$ increases, the differences in the force-extension curves between these boundary conditions become smaller. Here, the results have been plotted using $N = 100$ terms in Eqs. (54) and (55). To check convergence and accuracy, we estimated values of $\langle X\rangle/L$ for $F = 10$ pN and $\mathscr{A} = 1$. Summing $n = 10$, 20, 50, 90, and 100 terms, we find values $\langle X\rangle/L = 0.7696$, 0.7496, 0.7374, 0.7338, and 0.7333, confirming moderately rapid convergence and high accuracy.

B. Activity from experimental measurements

Experiments of fluctuating filaments in active media form an integral part of the biophysical characterization of active or biological materials. In many of these cases, the activity of the ambient medium may not be known quantitatively. Here, we discuss several ways of measuring the activity using expressions derived above. In each case, it is assumed that the thermal temperature of the bath T, the contour length of the polymer L, and the force exerted F are known. Properties of the active agents and the distribution of active sites encoded in ℓ are also assumed to be known along with drag and diffusion coefficients. For the specific case of a polymer in an active bath, these can be easily estimated from experiments without the polymer by visually tracking the self-propelling agents and computing correlation functions.

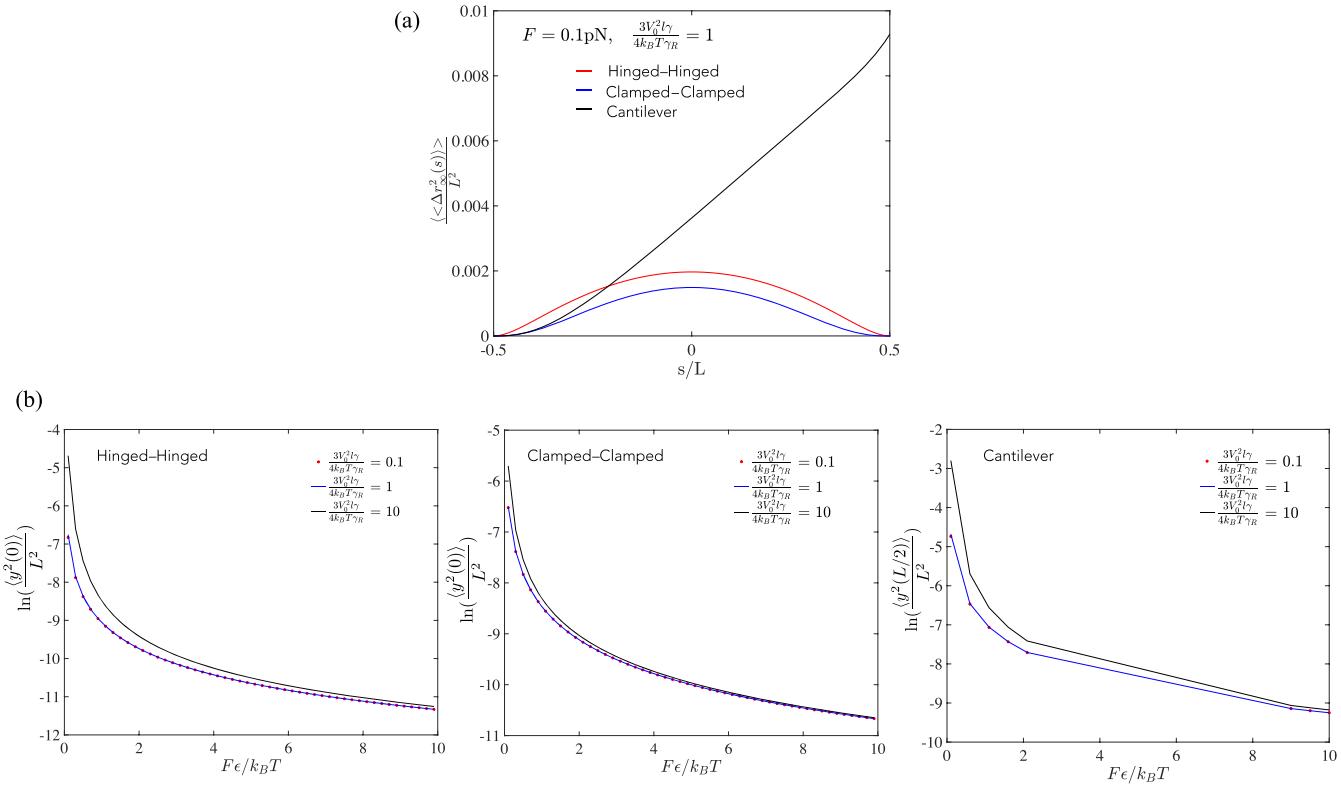

FIG. 3. (a) Mean square displacement for the different boundary conditions in the limit of small force. Parameters are ε = 17.1 μm, L = 8.54 μm, V_0 = 9.22 μm/s, ℓ = 7 nm, T = 300 K, γ_R = 0.16 s, and γ = 1.47 × 10^{-3} N s/m^2. (b) Here, we show the variation in the mean square lateral displacements at the central point s = 0 of the polymer filament as a function of the imposed extensional force for the clamped–clamped and hinged–hinged cases and at $s = L/2$ for the cantilever case.

Focusing on experiments conducted at a large force, we note that rewriting the asymptotic expansion obtained from Eq. (29) provides a relation between an effective bending modulus $\widetilde{K}_b$, the purely thermal bending modulus K_b, and V_0,

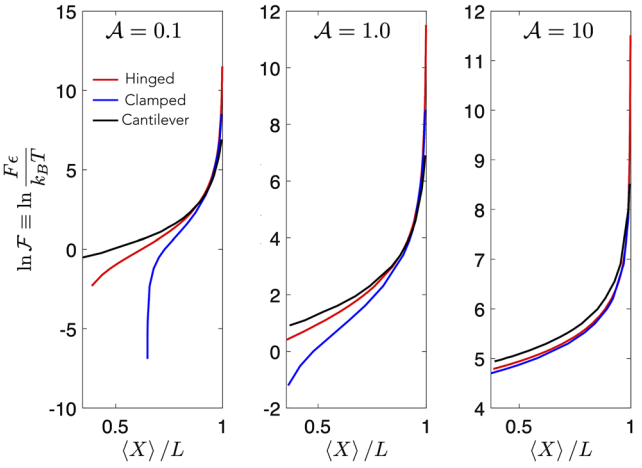

FIG. 4. Force-extension relations under three types of boundary conditions. The filament length used there is L = 68.2 μm. Other parameters are the same as Fig. 3.

$$1 - \frac{k_B T}{\sqrt{4\widetilde{K}_b F}} = 1 - \frac{1}{\sqrt{4K_b F}}\left(k_B T + \frac{3V_0^2 \ell\gamma}{4\gamma_R}\right). \tag{60}$$

The effective bending modulus, $\widetilde{K}_b$, here is defined as the apparent bending modulus in an active bath. We stipulate that this is the modulus deduced from a read-out of observed persistence lengths (including the effects of activity). We point out that Eq. (60) allows for extraction of information about the activity in a straightforward manner, provided the purely thermal modulus is known (perhaps from experiments in a passive thermally equilibrated bath).

From a knowledge of $\widetilde{K}_b$ and K_b, we can then determine the velocity V_0 representing the activity in the bath and/or filament,

$$V_0 = \sqrt{4\gamma_R k_B T\left(\sqrt{K_b/\widetilde{K}_b} - 1\right)/3\ell\gamma}. \tag{61}$$

Note that the use of Eq. (61) requires us to plug in values for the length scale ℓ and the friction coefficients γ and γ_R, which can be estimated by tagging the active agents/particles and measuring their single agent mean square displacements and re-orientation characteristics. This method is useful when the filament is long compared to its persistence length so that the end-to-end extension varies over broad range under various applied tensions.

In the case of clamped–clamped filaments, one could measure the mean square deflection at the center s = 0 of the filament in an

experiment to estimate V_0 using

$$\langle y^2(0)\rangle \approx \sum_{n=1}^{100} \varphi_n^2(0)\left[\frac{2k_B T\tau_n}{\gamma} + \frac{2V_0^2\ell\tau_n^2}{1+\gamma_R\tau_n}\right], \tag{62}$$

$$V_0^2 = \frac{\langle y^2(0)\rangle - \sum_{n=1}^{100}\varphi_n^2(0)\frac{2k_B T\tau_n}{\gamma}}{\sum_{n=1}^{100}\varphi_n^2(0)\frac{2\ell\tau_n^2}{1+\gamma_R\tau_n}}, \tag{63}$$

where eigenfunctions φ_n are given in Eqs. (51) and (53). Figure 5(a) shows non-dimensional mean squared deflections plotted against $\mathscr{A}$ for various values of the tension. From a knowledge of the mean square displacement, one can read the value of V_0 using these curves. It may even be possible to measure $\langle y^2(s)\rangle$ over the range $-L/2 \le s \le L/2$ for clamped–clamped or hinged–hinged boundary conditions

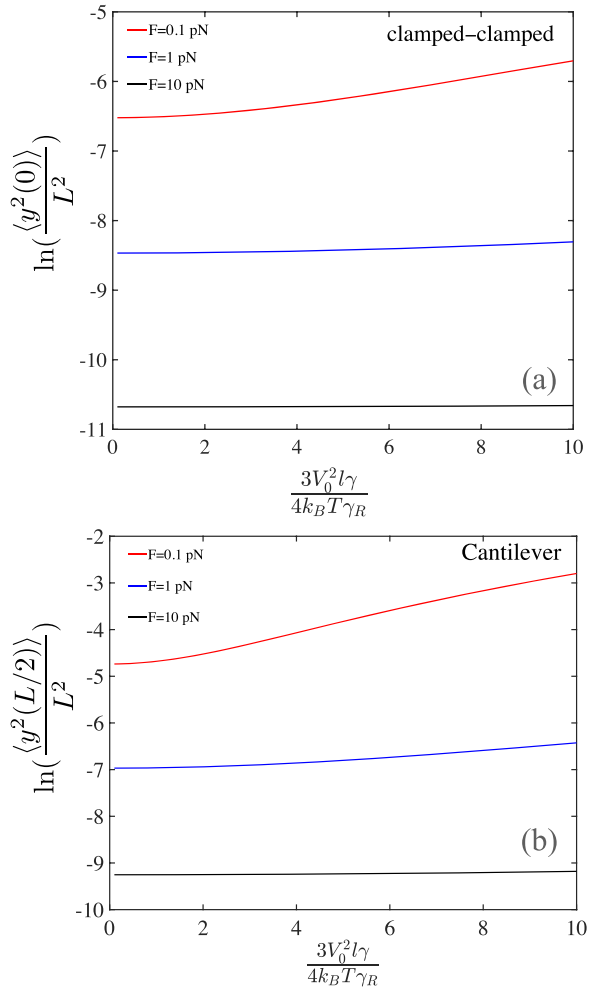

FIG. 5. (a) Dimensionless mean square displacement at $s = 0$ as a function of dimensionless propulsion velocity under different applied tension $F = 0.1$ pN, $F = 1$ pN, and $F = 10$ pN for a clamped–clamped filament. (b) Dimensionless mean square displacement at $s = L/2$ as a function of dimensionless propulsion velocity under different applied tension $F = 0.1$ pN, $F = 1$ pN, and $F = 10$ pN for a cantilevered filament. Other parameters are the same as in Fig. 3.

with known applied forces on filaments and known bending moduli as in the work of Arsenault *et al.*[47] (who applied forces using optical traps on actin filaments) and then fit the appropriate expressions with V_0 as the fitting parameter. This method is useful when the lengths of the filaments are comparable to their persistence length.

In the case of cantilevered filaments (as in tethered particle experiments), one could measure the mean square deflection at the right end $s = \frac{L}{2}$ of the filament to estimate V_0 using

$$\left\langle y^2\left(\frac{L}{2}\right)\right\rangle \approx \sum_{n=1}^{100}\varphi_n^2\left(\frac{L}{2}\right)\left[\frac{2k_B T\tau_n}{\gamma} + \frac{2V_0^2\ell\tau_n^2}{1+\gamma_R\tau_n}\right], \tag{64}$$

$$V_0^2 = \frac{\left\langle y^2\left(\frac{L}{2}\right)\right\rangle - \sum_{n=1}^{100}\varphi_n^2\left(\frac{L}{2}\right)\frac{2k_B T\tau_n}{\gamma}}{\sum_{n=1}^{100}\varphi_n^2\left(\frac{L}{2}\right)\frac{2\ell\tau_n^2}{1+\gamma_R\tau_n}}, \tag{65}$$

where eigenfunctions φ_n are given in Eq. (59). Figure 5(b) shows that the mean square deflection at the right end increases as the active agents increase under three different applied forces. However, this variation is not significant at large force (10 pN).

Here, we have exploited the influence of activity on fluctuations of a semi-flexible polymer to estimate V_0. Other ways of estimating V_0 exist. Indeed, tracking individual active agents such as bacterial cells in a suspension or by following the displacements and velocity fluctuations of tracer particles (see Ref. 23) allows us to extract the active diffusivity V_0^2/γ_R defined in Eq. (37) from which V_0 can be obtained. However, there are important physical situations when micro-scopic filaments are simultaneously under the action of thermal and active forces as in the cytoskeleton of a live cell. We have attempted to understand the force-extension relations and fluctuations of such filaments. By using our expressions for V_0, one may compute the strength of activity inside a live cell from visual observations such as obtained by florescence microscopy without introducing a disturbing probe in the cell's interior.

V. SUMMARY AND CONCLUSIONS

Filaments in live cells are subject to activity in addition to thermal Brownian motion. Furthermore, they may constitute a component of a networked structure or be subject to constraints through boundary conditions. Active filaments can be also synthetically manufactured by connecting polar and self-propelling colloids. In both these and more general cases, the stochastic noisy nature of filament configurations arises from thermal noise and from athermal noise—the latter may originate from the interaction of the polymer with surrounding active (Brownian) agents or from the inherent motion of the polymer itself, which may be composed of active agents.[48–51]

Here, starting from a description of an active noisy filament as a continuous Gaussian semi-flexible polymer, we study how it responds under tension when constrained. We analyze the deformation of filaments under three distinct boundary conditions—hinged–hinged, clamped–clamped, and a cantilever. Analytical expressions for the mean squared deflections and end-to-end distance (or mean stretch) of the polymer are derived, and their variation with respect to activity and the magnitude of the applied force are explored. The expressions for these quantities under hinged–hinged boundary conditions are reminiscent of the worm-like-chain

model with a modified temperature that depends on the characteristic velocity of the activity. Our results provide methods to estimate the activity (of filaments or bath) by measurements of the force-extension relation of the filaments or their mean square deflections, which can be routinely performed using optical traps, tethered particle experiments, or other single molecule techniques. We have attempted to understand the force-extension relations and fluctuations of such filaments.

We conclude by suggesting future extensions of our theoretical approach and applications in related active matter fields. First, we note that our analysis and theory may be extended to filaments fluctuating in three dimensions, provided the filaments/polymers are not subject to significant torsion. When bending deformations dominate, we can account for variations in the third dimension by incorporating the analysis in two perpendicular planes of deformation for each mode as described for the passive case in some of our previous work (see Purohit *et al.*[37] and Su and Purohit[38]). Second, at the multi-filament level such as for beds of active filaments or carpets of active filaments,[52–54] natural extensions of our approach may be to study the response to compression of a carpet or bed of wall-tethered active polymers. In this case, modifying the drag coefficients to depend on the local mean orientations of neighboring polymers will also allow for a minimal incorporation of inter-filament or inter-polymer interactions. Finally, our theoretical framework can be extended to problems that probe filament behavior in active suspensions or in natural or synthetic composites such as reconstituted filament-motor mixtures. Recent analysis of constrained active filaments animated by follower forces[52,53] such as induced by perfectly aligned molecular motors in microtubule and actin assays can be studied using an adaptation of Eq. (4). Similarly, the fluctuations of a spherical bead grafted or tethered to surfaces by a slender semi-flexible polymer embedded in an active fluid comprised of self-propelling agents such as bacterial swarms,[46,55] or photosensitive or phoretic colloidal suspensions, or in hierarchically assembled natural[56] and synthetic active matter[57] can also be used to quantify activity. The force exerted by the diffusing bead F on the filament is here a fluctuating force that varies on time scales controlled by collective flow and agent–bead interactions. Using a bead that is ~10 μm–20 μm allows one to sample not just individual bacteria but also collective velocity fields such as fluctuating vortices.[46,55]

ACKNOWLEDGMENTS

X.L. and P.K.P. acknowledge support for this work through Grant No. NSF-CMMI-1662101. A.G. acknowledges support for this work through NSF Grant No. NSF-MCB-2026782.

APPENDIX A: EQUATIONS SIMPLIFIED FURTHER IN THE MAIN TEXT

In this appendix, we provide the full expressions for equations that are either further simplified, analyzed using asymptotic methods, or evaluated numerically in the main narrative of this paper. For clarity, we have listed them here.

Equations for the mean-square displacement in the hinged–hinged case obtained (33)–(35) may be simplified further to obtain the general expression

$$\begin{aligned}\left\langle y^2(s)\right\rangle = \frac{1}{2L}\Bigg[&-\frac{c\pi\,\mathrm{csch}(\pi\sqrt{r_1})(\cosh(\pi\sqrt{r_1})-\cosh(2\pi\sqrt{r_1}s/L))}{r_1^{3/2}\sqrt{b^2-4ad}(b-ar_1)}\\&+\frac{c\pi\,\mathrm{csch}(\pi\sqrt{r_2})(\cosh(\pi\sqrt{r_2})-\cosh(2\pi\sqrt{r_2}s/L))}{r_2^{3/2}\sqrt{b^2-4ad}(b-ar_2)}\\&-\frac{c\pi^4\,\mathrm{csch}(\mathscr{L}_2)(\cosh(\mathscr{L}_2)-\cosh(2s\mathscr{L}_2/L))}{\mathscr{L}_2^3(b-ar_1)(b-ar_2)}\\&+\frac{\pi^2 c\left(1-4s^2/L^2\right)}{2bd}+\frac{k_\mathrm{B}\mathrm{T}L^2}{F}\\&\times\left(1-\frac{4\,s^2}{L^2}-\frac{2\mathrm{csch}\mathscr{L}_2(\cosh\mathscr{L}_2-\cosh(2\,s/\ell_\mathrm{f}))}{\mathscr{L}_2}\right)\Bigg].\end{aligned}\tag{A1}$$

Simplifying this provides the asymptotic expression (36) valid for large forces, $F\to\infty$. Similarly, the equation for the scaled stretch $\langle X\rangle/L$ can be obtained by reorganizing Eq. (38). We then get

$$\begin{aligned}\frac{\langle X\rangle}{L} =&\left[1+\frac{\varepsilon}{\mathscr{F}L}-\frac{\left(\sqrt{\mathscr{F}}L\coth\left(\frac{\sqrt{\mathscr{F}}L}{\varepsilon}\right)+\varepsilon\right)}{2\mathscr{F}L}\right]+\frac{c\varepsilon\left(L-\pi^2\sqrt{\frac{\mathscr{F}k_\mathrm{B}\mathrm{T}}{a\varepsilon}}\coth\left(\frac{\pi^2\sqrt{\frac{\mathscr{F}k_\mathrm{B}\mathrm{T}}{a\varepsilon}}}{L}\right)\right)}{4d\mathscr{F}k_\mathrm{B}\mathrm{T}L^2}\\&-\frac{\frac{c\pi^3}{\sqrt{a\varepsilon}}\sqrt{2\pi^2\mathscr{F}k_\mathrm{B}\mathrm{T}-2\varepsilon\sqrt{\frac{\pi^4\mathscr{F}^2(k_\mathrm{B}\mathrm{T})^2}{\varepsilon^2}-4adL^4}}\coth\left(\frac{\pi}{\sqrt{2a\varepsilon}L}\sqrt{\pi^2\mathscr{F}k_\mathrm{B}\mathrm{T}-\varepsilon\sqrt{\frac{\pi^4\mathscr{F}^2(k_\mathrm{B}\mathrm{T})^2}{\varepsilon^2}-4adL^4}}\right)}{8dL^4\sqrt{\frac{\pi^4\mathscr{F}^2(k_\mathrm{B}\mathrm{T})^2}{L^4\varepsilon^2}-4ad}}\\&+\frac{\frac{c\pi^3}{\sqrt{a\varepsilon}}\sqrt{2\pi^2\mathscr{F}k_\mathrm{B}\mathrm{T}+2\varepsilon\sqrt{\frac{\pi^4\mathscr{F}^2(k_\mathrm{B}\mathrm{T})^2}{\varepsilon^2}-4adL^4}}\coth\left(\frac{\pi}{\sqrt{2a\varepsilon}L}\sqrt{\pi^2\mathscr{F}k_\mathrm{B}\mathrm{T}+\varepsilon\sqrt{\frac{\pi^4\mathscr{F}^2(k_\mathrm{B}\mathrm{T})^2}{\varepsilon^2}-4adL^4}}\right)}{8dL^4\sqrt{\frac{\pi^4\mathscr{F}^2(k_\mathrm{B}\mathrm{T})^2}{L^4\varepsilon^2}-4ad}}.\end{aligned}\tag{A2}$$

For the clamped–clamped case derived in the main text [Eqs. (50)–(53)], constants κ_{1n} and κ_{2n} have the following closed forms:

$$\kappa_{1n} = \frac{1}{4\zeta_n\zeta_n'(\zeta_n^2+\zeta_n'^2)}\Big[20\zeta_n^2\zeta_n'^3\cot\Big(\frac{L\zeta_n}{2}\Big) + 4\zeta_n'^5\cot\Big(\frac{L\zeta_n}{2}\Big) + 2L\zeta_n\zeta_n'^5\csc^2\Big(\frac{L\zeta_n}{2}\Big) + 2\zeta_n^5\big(L\zeta_n' + \sinh\big(L\zeta_n'\big)\big)\operatorname{csch}^2\Big(\frac{L\zeta_n'}{2}\Big) + \zeta_n^3\zeta_n'^2\Big(20\coth\Big(\frac{L\zeta_n'}{2}\Big) - L\zeta_n'\csc^2\times\Big(\frac{L\zeta_n}{2}\Big)\operatorname{csch}^2\Big(\frac{L\zeta_n'}{2}\Big)\big(\cos(L\zeta_n) - \cosh\big(L\zeta_n'\big)\big)\Big)\Big], \tag{A3}$$

$$\kappa_{2n} = \frac{1}{4\zeta_n\zeta_n'(\zeta_n^2+\zeta_n'^2)}\Big[-20\zeta_n^2\zeta_n'^3\tan\Big(\frac{L\zeta_n}{2}\Big) - 4\zeta_n'^5\tan + \Big(\frac{L\zeta_n}{2}\Big) + 2L\zeta_n\zeta_n'^5\sec^2\Big(\frac{L\zeta_n}{2}\Big) + 2\zeta_n^5\big(\sinh\big(L\zeta_n'\big) - L\zeta_n'\big)\operatorname{sech}^2\Big(\frac{L\zeta_n'}{2}\Big) + \zeta_n^3\zeta_n'^2\Big(20\tanh\Big(\frac{L\zeta_n'}{2}\Big) - L\zeta_n'\sec^2\Big(\frac{L\zeta_n}{2}\Big)\operatorname{sech}^2\times\Big(\frac{L\zeta_n'}{2}\Big)\big(\cos(L\zeta_n) - \cosh\big(L\zeta_n'\big)\big)\Big)\Big]. \tag{A4}$$

Finally, Eqs. (57)–(59) that enter in the expression for the mean displacement for the cantilever boundary condition involve constants t_{2n}–t_{4n} that are evaluated using the expressions

$$t_{2n} = \left(\frac{-\zeta_n^2\sin(\zeta_nL) + \zeta_n'^2\sinh(\zeta_n'L)}{\zeta_n^2\cos(\zeta_nL) + \zeta_n'^2\cosh(\zeta_n'L)}\cdot\frac{\zeta_n' - \zeta_n}{\zeta_n' + \zeta_n} - \frac{\zeta_n^2\sin(\zeta_nL) + \zeta_n'^2\sinh(\zeta_n'L)}{\zeta_n^2\cos(\zeta_nL) + \zeta_n'^2\cosh(\zeta_n'L)}\right)t_{4n}, \tag{A5}$$

$$t_{2n}\big[K_b\big(\zeta_n^3\sin(\zeta_nL) - \zeta_n'^3\sinh(\zeta_n'L)\big) - F\big(-\zeta_n\sin(\zeta_nL) - \zeta_n'\sinh(\zeta_n'L)\big)\big] + t_{3n}\big[K_b\big(-\zeta_n^3\cos(\zeta_nL) + \zeta_n'^3\cosh(\zeta_n'L)\big) - F\big(\zeta_n\cos(\zeta_nL) + \zeta_n'\cosh(\zeta_n'L)\big)\big] + t_{4n}\big[K_b\big(-\zeta_n^3\cos(\zeta_nL) - \zeta_n'^3\cosh(\zeta_n'L)\big) - F\big(\zeta_n\cos(\zeta_nL) - \zeta_n'\cosh(\zeta_n'L)\big)\big] = 0, \tag{A6}$$

$$\left(\frac{-\zeta_n^2\sin(\zeta_nL) + \zeta_n'^2\sinh(\zeta_n'L)}{\zeta_n^2\cos(\zeta_nL) + \zeta_n'^2\cosh(\zeta_n'L)}\cdot\frac{\zeta_n' - \zeta_n}{\zeta_n' + \zeta_n} - \frac{\zeta_n^2\sin(\zeta_nL) + \zeta_n'^2\sinh(\zeta_n'L)}{\zeta_n^2\cos(\zeta_nL) + \zeta_n'^2\cosh(\zeta_n'L)}\right)\cdot\big[K_b\big(\zeta_n^3\sin(\zeta_nL) - \zeta_n'^3\sinh(\zeta_n'L)\big) - F\big(-\zeta_n\sin(\zeta_nL) - \zeta_n'\sinh(\zeta_n'L)\big)\big] + \left(\frac{\zeta_n' - \zeta_n}{\zeta_n' + \zeta_n}\right)\cdot\big[K_b\big(-\zeta_n^3\cos(\zeta_nL) + \zeta_n'^3\cosh(\zeta_n'L)\big) - F\big(\zeta_n\cos(\zeta_nL) + \zeta_n'\cosh(\zeta_n'L)\big)\big] + \big[K_b\big(-\zeta_n^3\cos(\zeta_nL)\big) - \zeta_n'^3\cosh(\zeta_n'L) - F\big(\zeta_n\cos(\zeta_nL) - \zeta_n'\cosh(\zeta_n'L)\big)\big] = 0. \tag{A7}$$

APPENDIX B: HINGED–HINGED

Combining boundary conditions [Eq. (30)] with Eq. (12), we get four constraint equations

$$e^{\zeta_n'\frac{L}{2}}c_{1n} + e^{-\zeta_n'\frac{L}{2}}c_{2n} + \cos\zeta_n\frac{L}{2}c_{3n} + \sin\zeta_n\frac{L}{2}c_{4n} = 0, \tag{B1}$$

$$e^{-\zeta_n'\frac{L}{2}}c_{1n} + e^{\zeta_n'\frac{L}{2}}c_{2n} + \cos\zeta_n\frac{L}{2}c_{3n} - \sin\zeta_n\frac{L}{2}c_{4n} = 0, \tag{B2}$$

$$e^{\zeta_n'\frac{L}{2}}c_{1n} + e^{-\zeta_n'\frac{L}{2}}c_{2n} - \frac{\zeta_n^2}{\zeta_n'^2}\cos\zeta_n\frac{L}{2}c_{3n} - \frac{\zeta_n^2}{\zeta_n'^2}\sin\zeta_n\frac{L}{2}c_{4n} = 0, \tag{B3}$$

$$e^{-\zeta_n'\frac{L}{2}}c_{1n} + e^{\zeta_n'\frac{L}{2}}c_{2n} - \frac{\zeta_n^2}{\zeta_n'^2}\cos\zeta_n\frac{L}{2}c_{3n} + \frac{\zeta_n^2}{\zeta_n'^2}\sin\zeta_n\frac{L}{2}c_{4n} = 0. \tag{B4}$$

Comparing the expressions Eqs. (B1)–(B3) and Eqs. (B2)–(B4) (here "–" means subtract), we deduce that

$$c_{1n} = c_{2n} = \cos\zeta_n\frac{L}{2}c_{3n} = \sin\zeta_n\frac{L}{2}c_{4n} = 0. \tag{B5}$$

This indicates two sets of solutions

$$c_{1n} = c_{2n} = c_{4n} = 0,\quad \zeta_n = \frac{1+2n}{L}\pi,\qquad \varphi_n(s) = c_{3n}\cos\frac{1+2n}{L}\pi s, \tag{B6}$$

and

$$c_{1n} = c_{2n} = c_{3n} = 0,\quad \zeta_n = \frac{2n}{L}\pi,\qquad \varphi_n(s) = c_{4n}\sin\frac{2n}{L}\pi s. \tag{B7}$$

The general solution of $\varphi_n(s)$ could be obtained immediately through the combination of Eqs. (B6) and (B8) as well as the constraint $\|\varphi_n(s)\|_{L^2} = 1$,

$$\varphi_n(s) = \sqrt{\frac{2}{L}}\sin\Big(\frac{n\pi s}{L} + \frac{n\pi}{2}\Big). \tag{B8}$$

The first term in Eq. (33) can be summed as in Ref. 37, and the result is

$$\sum_{n=1}^{\infty}\frac{2}{L}\sin^2\left(\frac{n\pi s}{L}+\frac{n\pi}{2}\right)\frac{2k_{\mathrm{B}}\mathrm{T}\tau_n}{\gamma} = \frac{L^3}{2\varepsilon\mathscr{L}_2^2}\left[\left(1-\frac{4s^2}{L^2}\right)-\frac{\cosh(\mathscr{L}_2)-\cosh(2\mathscr{L}_2 s/L)}{\frac{\mathscr{L}_2}{2}\sinh(\mathscr{L}_2)}\right]. \quad \text{(B9)}$$

In order to compute the second term in Eq. (33), we introduce for brevity

$$x=n^2,\quad a=\frac{k_{\mathrm{B}}\mathrm{T}\varepsilon\pi^4}{L^4},\quad b=\frac{F}{L^2}\pi^2,\quad c=2V_0^2 l\gamma^2,\quad d=\gamma_R\gamma,$$

$$b=\frac{F}{L^2}\pi^2,\quad c=2V_0^2 l\gamma^2,\quad d=\gamma_R\gamma.$$

Using x_1 and x_2 as defined, we obtain

$$x_1=\frac{-b+\sqrt{b^2-4ad}}{2a},\quad x_2=\frac{-b-\sqrt{b^2-4ad}}{2a},$$

$$\frac{2V_0^2 l\tau_n^2}{1+\gamma_R\tau_n} = \frac{2V_0^2 l\gamma^2}{n^4\left(k_{\mathrm{B}}\mathrm{T}\frac{\varepsilon\pi^4}{L^4}n^2+F\frac{\pi^2}{L^2}\right)^2+\gamma_R\gamma\left(k_{\mathrm{B}}\mathrm{T}\frac{\varepsilon\pi^4}{L^4}n^2+F\frac{\pi^2}{L^2}\right)n^2} = \frac{c}{b}\left(\frac{1}{x}-\frac{a}{ax+b}\right)\frac{1}{ax^2+bx+d}, \quad \text{(B10)}$$

$$\begin{aligned}\frac{2V_0^2 l\tau_n^2}{1+\gamma_R\tau_n} &= \frac{c}{ab}\left(\frac{1}{x}-\frac{1}{x+\frac{b}{a}}\right)\left(\frac{1}{x-x_1}-\frac{1}{x-x_2}\right)\frac{a}{\sqrt{b^2-4ad}}\\ &= \frac{c}{b\sqrt{b^2-4ad}}\left[\left(\frac{1}{x-x_1}-\frac{1}{x}\right)\frac{1}{x_1}+\left(\frac{1}{x+\frac{b}{a}}-\frac{1}{x-x_1}\right)\frac{1}{x_1+\frac{b}{a}}+\left(\frac{1}{x}-\frac{1}{x-x_2}\right)\frac{1}{x_2}+\left(\frac{1}{x-x_2}-\frac{1}{x+\frac{b}{a}}\right)\frac{1}{\frac{b}{a}+x_2}\right]\\ &= \frac{c}{b\sqrt{b^2-4ad}}\left[\frac{b}{a}\frac{1}{x_1^2+\frac{b}{a}x_1}\frac{1}{x-x_1}+\frac{\sqrt{b^2-4ad}}{d}\frac{1}{x}+\frac{-\frac{b}{a}}{(\frac{b}{a}+x_2)x_2}\frac{1}{x-x_2}+\frac{-\frac{\sqrt{b^2-4ad}}{a}}{(x_1+\frac{b}{a})(x_2+\frac{b}{a})}\frac{1}{x+\frac{b}{a}}\right].\end{aligned} \quad \text{(B11)}$$

The second term in Eq. (33) can be simplified further using

$$\sum_{n=0}^{\infty}\frac{(-1)^n\varepsilon_n}{n^2+z^2}\cos(2n\pi s/L)=\frac{\pi}{z}\frac{\cosh(2\pi z s/L)}{\sinh(\pi z)}, \quad \forall z\in\mathbb{C},\ \varepsilon_0=1,\varepsilon_n=2,n\geq 1, \quad \text{(B12)}$$

$$\begin{aligned}&\sum_{n=1}^{\infty}\frac{2}{L}\left(\frac{1}{2}-\frac{1}{2}\cos\left(\frac{2n\pi s}{L}\right)(-1)^n\right)\frac{2V_0^2 l\tau_n^2}{1+\gamma_R\tau_n}\\ &= \frac{2}{L}\frac{c}{a\sqrt{b^2-4ad}(x_1^2+\frac{b}{a}x_1)}\left[\frac{1}{4}\left(\cosh(\pi\sqrt{-x_1})-\cosh\left(\frac{2\pi\sqrt{-x_1}s}{L}\right)\right)\cdot\frac{\pi}{\sqrt{-x_1}\sinh(\pi\sqrt{-x_1})}\right]\\ &-\frac{2}{L}\frac{c}{a\sqrt{b^2-4ad}(x_2^2+\frac{b}{a}x_2)}\left[\frac{1}{4}\frac{\pi}{\sqrt{-x_2}\sinh(\pi\sqrt{-x_2})}\cdot\left(\cosh(\pi\sqrt{-x_2})-\cosh\left(\frac{2\pi\sqrt{-x_2}s}{L}\right)\right)\right]\\ &-\frac{2}{L}\frac{c}{ab}\frac{1}{(x_1+\frac{b}{a})(x_2+\frac{b}{a})}\left[\frac{1}{4}\frac{\pi}{\sqrt{b/a}\sinh\left(\pi\sqrt{b/a}\right)}\cdot\left(\cosh\left(\pi\sqrt{\frac{b}{a}}\right)-\cosh\left(\frac{2\pi\sqrt{b/a}s}{L}\right)\right)\right]+\frac{\pi^2L^2c-4\pi^2cs^2}{4L^3bd}.\end{aligned} \quad \text{(B13)}$$

Setting $r_1=-x_1$, $r_2=-x_2$, Eq. (26) can be summed to obtain Eq. (A1). Let $\delta=(d/a)^{\frac{1}{4}}$. For the force-extension relation, in the limit of $\mathscr{F}\to 0$, we obtain

$$\begin{aligned}\frac{\langle X\rangle}{L} &= 1-\left[\frac{L}{6\varepsilon}+\frac{\pi^4 c}{12adL^3}-\frac{\sqrt{2}\pi^3 c}{8adL^3\delta}\frac{\sin(\sqrt{2}\pi\delta)-\sinh(\sqrt{2}\pi\delta)}{\cos(\sqrt{2}\pi\delta)-\cosh(\sqrt{2}\pi\delta)}\right]+o(\mathscr{F})+\frac{\mathscr{F}}{1440a^2d^2L^5\varepsilon^2}\\ &\times\left[16a^2d^2L^8\frac{1}{\varepsilon}+\left(8d\pi^8k_{\mathrm{B}}\mathrm{T}\varepsilon+180\pi^6k_{\mathrm{B}}\mathrm{T}\varepsilon\sqrt{ad}\frac{\sin(\sqrt{2}\pi\delta)\sinh(\sqrt{2}\pi\delta)}{\left(\cos(\sqrt{2}\pi\delta)-\cosh(\sqrt{2}\pi\delta)\right)^2}+45\sqrt{2}\pi^5 ak_{\mathrm{B}}\mathrm{T}\varepsilon\delta\frac{\sin(\sqrt{2}\pi\delta)+\sinh(\sqrt{2}\pi\delta)}{\left(\cos(\sqrt{2}\pi\delta)-\cosh(\sqrt{2}\pi\delta)\right)^2}\right)c\right].\end{aligned} \quad \text{(B14)}$$

APPENDIX C: CLAMPED–CLAMPED

After dragging Eq. (49) into Eq. (15), we have

$$\begin{bmatrix} e^{\zeta'_n\frac{L}{2}} & e^{-\zeta'_n\frac{L}{2}} & \cos\zeta_n\frac{L}{2} & \sin\zeta_n\frac{L}{2} \\ e^{-\zeta'_n\frac{L}{2}} & e^{\zeta'_n\frac{L}{2}} & \cos\zeta_n\frac{L}{2} & -\sin\zeta_n\frac{L}{2} \\ \zeta'_n e^{\zeta'_n\frac{L}{2}} & -\zeta'_n e^{-\zeta'_n\frac{L}{2}} & -\zeta_n\sin\zeta_n\frac{L}{2} & \zeta_n\cos\zeta_n\frac{L}{2} \\ \zeta'_n e^{-\zeta'_n\frac{L}{2}} & -\zeta'_n e^{\zeta'_n\frac{L}{2}} & \zeta_n\sin\zeta_n\frac{L}{2} & \zeta_n\cos\zeta_n\frac{L}{2} \end{bmatrix} \begin{bmatrix} d_{1n} \\ d_{2n} \\ d_{3n} \\ d_{4n} \end{bmatrix} = \mathbf{0}. \tag{C1}$$

Using the Gaussian elimination, the coefficient matrix in Eq. (C1) can be simplified to

$$\begin{aligned} &\begin{bmatrix} & 1 & 1 & \\ 1 & -1 & & \\ & & 1 & -1 \\ 1 & 1 & & \end{bmatrix} \begin{bmatrix} 1 & -1 & & \\ & 1 & & -1 \\ 1 & & 1 & \\ & 1 & & 1 \end{bmatrix} \begin{bmatrix} 1 & 1 & & \\ 1 & -1 & & \\ & & 1 & 1 \\ & & 1 & -1 \end{bmatrix} \cdot \begin{bmatrix} e^{\zeta'_n\frac{L}{2}} & e^{-\zeta'_n\frac{L}{2}} & \cos\zeta_n\frac{L}{2} & \sin\zeta_n\frac{L}{2} \\ e^{-\zeta'_n\frac{L}{2}} & e^{\zeta'_n\frac{L}{2}} & \cos\zeta_n\frac{L}{2} & -\sin\zeta_n\frac{L}{2} \\ \zeta'_n e^{\zeta'_n\frac{L}{2}} & -\zeta'_n e^{-\zeta'_n\frac{L}{2}} & -\zeta_n\sin\zeta_n\frac{L}{2} & \zeta_n\cos\zeta_n\frac{L}{2} \\ \zeta'_n e^{-\zeta'_n\frac{L}{2}} & -\zeta'_n e^{\zeta'_n\frac{L}{2}} & \zeta_n\sin\zeta_n\frac{L}{2} & \zeta_n\cos\zeta_n\frac{L}{2} \end{bmatrix} \\ &= \begin{bmatrix} 2\left(\cosh\zeta'_n\frac{L}{2}+\sinh\zeta'_n\frac{L}{2}\right) & 0 & \cos\zeta_n\frac{L}{2}-\sin\zeta_n\frac{L}{2}\frac{\zeta_n}{\zeta'_n} & \frac{\zeta_n}{\zeta'_n}\cos\zeta_n\frac{L}{2}+\sin\zeta_n\frac{L}{2} \\ 0 & 2\left(\cosh\zeta'_n\frac{L}{2}+\sinh\zeta'_n\frac{L}{2}\right) & \cos\zeta_n\frac{L}{2}-\sin\zeta_n\frac{L}{2}\frac{\zeta_n}{\zeta'_n} & -\frac{\zeta_n}{\zeta'_n}\cos\zeta_n\frac{L}{2}-\sin\zeta_n\frac{L}{2} \\ 2\left(\cosh\zeta'_n\frac{L}{2}-\sinh\zeta'_n\frac{L}{2}\right) & 0 & \cos\zeta_n\frac{L}{2}+\sin\zeta_n\frac{L}{2}\frac{\zeta_n}{\zeta'_n} & \frac{\zeta_n}{\zeta'_n}\cos\zeta_n\frac{L}{2}-\sin\zeta_n\frac{L}{2} \\ 0 & 2\left(\cosh\zeta'_n\frac{L}{2}-\sinh\zeta'_n\frac{L}{2}\right) & \cos\zeta_n\frac{L}{2}+\sin\zeta_n\frac{L}{2}\frac{\zeta_n}{\zeta'_n} & -\frac{\zeta_n}{\zeta'_n}\cos\zeta_n\frac{L}{2}+\sin\zeta_n\frac{L}{2} \end{bmatrix} \triangleq \begin{bmatrix} A & 0 & B & C \\ 0 & A & B & -C \\ D & 0 & E & F \\ 0 & D & E & -F \end{bmatrix}. \end{aligned} \tag{C2}$$

Applying Gaussian elimination once more on Eq. (C2), we get

$$\begin{aligned} &\begin{bmatrix} 1 & 1 & & \\ 1 & -1 & & \\ & & 1 & 1 \\ & & 1 & -1 \end{bmatrix} \begin{bmatrix} A & 0 & B & C \\ 0 & A & B & -C \\ D & 0 & E & F \\ 0 & D & E & -F \end{bmatrix} = \begin{bmatrix} A & A & 2B & 0 \\ D & D & 2E & 0 \\ A & -A & 0 & 2C \\ D & -D & 0 & 2F \end{bmatrix} \\ &\Longrightarrow \begin{bmatrix} A & A & 2B & 0 \\ D & D & 2E & 0 \\ A & -A & 0 & 2C \\ D & -D & 0 & 2F \end{bmatrix} \begin{bmatrix} d_{1n} \\ d_{2n} \\ d_{3n} \\ d_{4n} \end{bmatrix} = \mathbf{0}. \end{aligned} \tag{C3}$$

It clearly follows from Eq. (C3) that in order to derive non-zero solutions, the only two possible cases are $AE = BD$, $AF \neq CD$ and $AE \neq BD$, $AF = CD$. To see this, note that if $AE \neq BD$, $AF \neq CD$, then $d_{1n} + d_{2n} = d_{3n} = d_{1n} - d_{2n} = d_{4n} = 0$, $\Rightarrow d_{1n} = d_{2n} = d_{3n} = d_{4n} = 0$. Contradiction. If $AE = BD$, $AF = CD$, we will get $\cosh\zeta'_n\frac{L}{2}\sin\zeta_n\frac{L}{2} = 0$ & $\sinh\zeta'_n\frac{L}{2}\cos\zeta_n\frac{L}{2} = 0 \Longrightarrow \sin\zeta_n\frac{L}{2} = \cos\zeta_n\frac{L}{2} = 0$. Contradiction. Now, if $AE = BD$, $AF \neq CD$, then $d_{1n} = d_{2n}, d_{3n} = -\frac{Ad_{1n}}{B}, d_{4n} = 0$, and we get Eq. (51). Similarly, if $AE \neq BD$, $AF = CD$, then $d_{1n} = -d_{2n}$, $d_{3n} = 0$, $d_{4n} = -Ad_{1n}/C$, and we get Eq. (53).

DATA AVAILABILITY

The data that support the findings of this study are available within the article.

REFERENCES

[1] M. Fixman and J. Kovac, "Polymer conformational statistics III: Modified Gaussian models of the stiff chains," J. Chem. Phys. **58**, 1564–1568 (1973).
[2] C. Bustamante, J. Marko, E. Siggia, and S. Smith, "Entropic elasticity of Lambda phage DNA," Science **265**, 1599–1600 (1994).
[3] C. Bustamante, Z. Bryant, and S. B. Smith, "Ten years of tension: Single- molecule DNA mechanics," Nature **421**, 423–427 (2003).
[4] M. Radmacher, "Measuring the elastic properties of biological samples with the AFM," IEEE Eng. Med. Biol. Mag. **16**, 47–57 (1997).
[5] F. Gittes, B. Mickey, J. Nettleton, and J. Howard, "Flexural rigidity of microtubules and actin filaments measured from thermal fluctuations in shape," J. Cell Biol. **120**, 923–934 (1993).
[6] C. Bouchiat, M. D. Wang, J.-F. Allemand, T. Strick, S. M. Block, and V. Croquette, "Estimating the persistence length of a worm-like chain molecule from force-extension measurements," Biophys. J. **76**, 409–413 (1999).
[7] S. Smith, L. Finzi, and C. Bustamante, "Direct mechanical measurements of the elasticity of single DNA molecules by using magnetic beads," Science **258**, 1122–1126 (1992).
[8] M. D. Wang, H. Yin, R. Landick, J. Gelles, and S. M. Block, "Stretching DNA with optical tweezers," Biophys. J. **72**, 1335–1346 (1997).
[9] T. Yanagida, M. Nakase, K. Nishiyama, and F. Oosawa, "Direct observation of motion of single F-actin filaments in the presence of myosin," Nature **307**, 58–60 (1984).
[10] R. Phillips, J. Kondev, J. Theriot, and H. G. Garcia, *Physical Biology of the Cell*, 2nd ed. (Garland Science, 2013).
[11] A. Vaziri and A. Gopinath, "Cell and biomolecular mechanics in silico," Nat. Mater. **7**, 15–23 (2008).
[12] A. Marantan and L. Mahadevan, "Mechanics and statistics of the worm-like chain," Am. J. Phys. **86**, 86–94 (2018).
[13] A. Ghosh and N. S. Gov, "Dynamics of active semiflexible polymers," Biophys. J. **107**, 1065–1073 (2014).
[14] I. Jain, M. M. Inamdar, and R. Padinhateeri, "Statistical mechanics provides novel insights into microtubule stability and mechanism of shrinkage," PLoS Comput. Biol. **11**, e1004099 (2015).
[15] P. A. Wiggins, T. van der Heijden, F. Moreno-Herrero, A. Spakowitz, R. Phillips, J. Widom, C. Dekker, and P. C. Nelson, "High flexibility of dna on short length scales probed by atomic force microscopy," Nat. Nanotechnol. **1**, 137 (2006).
[16] P. A. Wiggins and P. C. Nelson, "Generalized theory of semiflexible polymers," Phys. Rev. E **73**, 031906 (2006).
[17] J. Weber, "Fluctuation dissipation theorem," Phys. Rev. **101**, 1620–1626 (1956).

[18]B. U. Felderhof, "On the derivation of the fluctuation-dissipation theorem," J. Phys. A: Math. Gen. **11**, 921–927 (1978).
[19]L. D. Landau and E. M. Lifshitz, *Course of Theoretical Physics*, 3rd ed. (Elsevier, 1980), p. 5.
[20]J. Palacci, S. Sacanna, S.-H. Kim, G.-R. Yi, D. J. Pine, and P. M. Chaikin, "Light-activated self-propelled colloids," Philos. Trans. R. Soc. A **372**, 20130372 (2014).
[21]R. E. Isele-Holder, J. Jäger, G. Saggiorato, J. Elgeti, and G. Gompper, "Dynamics of self-propelled filaments pushing a load," Soft Matter **12**, 8495–8505 (2016).
[22]M. W. Hahn, E. R. B. Moore, and M. G. Höfle, "Bacterial filament formation: A defense mechanism against flagellate grazing, is growth rate controlled in bacteria of different phyla," Appl. Environ. Microbiol. **65**, 25–35 (1999).
[23]A. E. Patteson, A. Gopinath, P. K. Purohit, and P. E. Arratia, "Particle diffusion in active fluids is non-monotonic in size," Soft Matter **12**, 2365–2372 (2016).
[24]A. E. Patteson, A. Gopinath, M. Goulian, and P. E. Arratia, "Running and tumbling with *E. coli* in polymeric solutions," Sci. Rep. **5**, 15761 (2015).
[25]A. E. Patteson, A. Gopinath, and P. E. Arratia, "Active colloids in complex fluids," Curr. Opin. Colloid Interface Sci. **21**, 86–93 (2016).
[26]T.-C. Lee, M. Alarcón-Correa, C. Miksch, K. Hahn, J. G. Gibbs, and P. Fischer, "Self-propelling nanomotors in the presence of strong Brownian forces," Nano Lett. **14**, 2407–2412 (2014).
[27]C. P. Brangwynne, G. H. Koenderink, F. C. MacKintosh, and D. A. Weitz, "Nonequilibrium microtubule fluctuations in a model cytoskeleton," Phys. Rev. Lett. **100**, 118104 (2008).
[28]E. Ben-Isaac, Y. Park, G. Popescu, F. L. Brown, N. S. Gov, and Y. Shokef, "Effective temperature of red-blood-cell membrane fluctuations," Phys. Rev. Lett. **106**, 238103 (2011).
[29]L. Harnau, R. G. Winkler, and P. Reineker, "Dynamic properties of molecular chains with variable stiffness," J. Chem. Phys. **102**, 7750–7757 (1995).
[30]T. Eisenstecken, G. Gompper, and R. Winkler, "Conformational properties of active semiflexible polymers," Polymers **8**, 304 (2016).
[31]T. Eisenstecken, G. Gompper, and R. G. Winkler, "Internal dynamics of semiflexible polymers with active noise," J. Chem. Phys. **146**, 154903 (2017).
[32]R. G. Winkler, P. Reineker, and L. Harnau, "Models and equilibrium properties of stiff molecular chains," J. Chem. Phys. **101**, 8119–8129 (1994).
[33]L. Harnau, R. G. Winkler, and P. Reineker, "Dynamic structure factor of semiflexible macromolecules in dilute solution," J. Chem. Phys. **104**, 6355–6368 (1996).
[34]L. Harnau, R. G. Winkler, and P. Reineker, "Influence of stiffness on the dynamics of macromolecules in a melt," J. Chem. Phys. **106**, 2469–2476 (1997).
[35]R. G. Winkler and G. Gompper, "The physics of active polymers and filaments," J. Chem. Phys. **153**, 040901 (2020).
[36]A. Martin-Gomez, T. Eisenstecken, G. Gompper, and R. G. Winkler, "Hydrodynamics of polymers in an active bath," Phys. Rev. E **101**, 052612 (2020).
[37]P. K. Purohit, M. E. Arsenault, Y. Goldman, and H. H. Bau, "The mechanics of short rod-like molecules in tension," Int. J. Non-Linear Mech. **43**, 1056–1063 (2008).
[38]T. Su and P. K. Purohit, "Thermomechanics of a heterogeneous fluctuating chain," J. Mech. Phys. Solids **58**, 164–186 (2010).
[39]J. Elgeti, R. G. Winkler, and G. Gompper, "Physics of microswimmers—Single particle motion and collective behavior: A review," Rep. Prog. Phys. **78**, 056601 (2015).
[40]M. C. Marchetti, Y. Fily, S. Henkes, A. Patch, and D. Yllanes, "Minimal model of active colloids highlights the role of mechanical interactions in controlling the emergent behavior of active matter," Curr. Opin. Colloid Interface Sci. **21**, 34–43 (2016).
[41]R. Winkler, S. Keller, and J. Rädler, "Intramolecular dynamics of linear macromolecules by fluorescence correlation spectroscopy," Phys. Rev. E **73**, 041919 (2006).
[42]A. Sangani and A. Gopinath, "Active Brownian particles and run-and-tumble particles: A comparative study," Eur. Phys. J. Spec. Top. **224**, 1231–1262 (2015).
[43]D. Loi, S. Mossa, and L. F. Cugliandolo, "Effective temperature of active complex matter," Soft Matter **7**, 3726–3729 (2011).
[44]A. Gopinath and D. L. Koch, "Collision and rebound of small droplets in an incompressible continuum gas," J. Fluid Mech. **454**, 145–201 (2002).
[45]A. Gopinath and D. L. Koch, "Dynamics of droplet rebound from a weakly deformable gas–liquid interface," Phys. Fluids **13**, 3526–3532 (2001).
[46]A. E. Patteson, A. Gopinath, and P. E. Arratia, "The propagation of active-passive interfaces in bacterial swarms," Nat. Commun. **9**, 5373 (2018).
[47]M. E. Arsenault, P. K. Purohit, Y. E. Goldman, H. Shuman, and H. H. Bau, "Comparison of Brownian-dynamics-based estimates of polymer tension with direct force measurements," Phys. Rev. E **82**, 051923 (2010).
[48]D. Nishiguchi, J. Iwasawa, H.-R. Jiang, and M. Sano, "Flagellar dynamics of chains of active Janus particles fueled by an AC electric field," New J. Phys. **20**, 015002 (2018).
[49]Z. Lin, T. Si, Z. Wu, C. Gao, X. Lin, and Q. He, "Light-activated active colloid ribbons," Angew. Chem., Int. Ed. **56**, 13517–13520 (2017).
[50]Y. Hong, N. M. Blackman, N. D. Kopp, A. Sen, and D. Velegol, "Chemotaxis of nonbiological colloidal rods," Phys. Rev. Lett. **99**, 178103 (2007).
[51]V. Garcia-Gradilla, J. Orozco, S. Sattayasamitsathit, F. Soto, F. Kuralay, A. Pourazary, A. Katzenberg, W. Gao, Y. Shen, and J. Wang, "Functionalized ultrasound-propelled magnetically guided nanomotors: Toward practical biomedical applications," ACS Nano **7**, 9232–9240 (2013).
[52]Y. Fily, P. Subramanian, T. M. Schneider, R. Chelakkot, and A. Gopinath, "Instabilities and spatiotemporal dynamics of active elastic filaments," J. R. Soc. Interface **17**, 20190794 (2020).
[53]R. Chelakkot, A. Gopinath, L. Mahadevan, and M. F. Hagan, "Flagellar dynamics of a connected chain of active, polar, Brownian particles," J. R. Soc. Interface **11**, 20130884 (2014).
[54]A. Sangani and A. Gopinath, "Elastohydrodynamical instabilities of active filaments, arrays, and carpets analyzed using slender-body theory," Phys. Rev. Fluids **5**, 083101 (2020).
[55]J. Yang, P. E. Arratia, A. E. Patteson, and A. Gopinath, "Quenching active swarms: Effects of light exposure on collective motility in swarming Serratia marcescens," J. R. Soc. Interface **16**, 20180960 (2019).
[56]T. Sanchez, D. T. N. Chen, S. J. DeCamp, M. Heymann, and Z. Dogic, "Spontaneous motion in hierarchically assembled active matter," Nature **491**, 431–434 (2012).
[57]M. S. Aporvari, M. Utkur, E. U. Saritas, G. Volpe, and J. Stenhammar, "Anisotropic dynamics of a self-assembled colloidal chain in an active bath," Soft Matter **16**, 5609 (2020).